JOURNAL OF GEOPHYSICAL RESEARCH, VOL. 113, B07110, doi:10.1029/2007JB005527, 2008

Deep-tow magnetic anomaly study of the Pacific Jurassic Quiet Zone and implications for the geomagnetic polarity reversal timescale and geomagnetic field behavior

Masako Tominaga,[1] William W. Sager,[1] Maurice A. Tivey,[2] and Sang-Mook Lee[3]

Received 27 November 2007; revised 16 April 2008; accepted 6 May 2008; published 26 July 2008.

[1] The Jurassic Quiet Zone (JQZ) is a region of low-amplitude magnetic anomalies whose distinctive character may be related to geomagnetic field behavior. We collected deep-tow magnetic profiles in Pigafetta Basin (western Pacific) where previous deep-tow data partially covered the JQZ sequence. Our goals were to extend the survey through the JQZ, examine anomaly correlations, and refine a preliminary geomagnetic polarity timescale (GPTS) model. We collected a series of closely spaced profiles over anomaly M34 and Ocean Drilling Program Hole 801C to examine anomaly correlation in detail, one profile in between previous profiles, and two long profiles extending the survey deeper into the JQZ. Anomaly features can be readily correlated except in a region of low-amplitude, short-wavelength anomalies in the middle of the survey area (''low-amplitude zone'' or LAZ). The small multiprofile surveys demonstrate anomaly linearity, implying that surrounding anomalies are also linear and likely result from crustal recording of geomagnetic field changes. We constructed a GPTS model assuming that most anomalies result from polarity reversals. The polarity timescale is similar to the polarity sequences from previous studies, but its global significance is uncertain because of problems correlating anomalies in the LAZ and the ambiguous nature of the small JQZ anomalies. Overall anomaly amplitude decreases with age into the LAZ and then increases again, implying low geomagnetic field strength, perhaps related to a rapidly reversing field. Other factors that may contribute to the LAZ are interference of anomalies over narrow, crustal polarity zones and poorly understood local tectonic complexities.

Citation: Tominaga, M., W. W. Sager, M. A. Tivey, and S.-M. Lee (2008), Deep-tow magnetic anomaly study of the Pacific Jurassic Quiet Zone and implications for the geomagnetic polarity reversal timescale and geomagnetic field behavior, *J. Geophys. Res.*, *113*, B07110, doi:10.1029/2007JB005527.

1. Introduction

[2] The Jurassic period appears to be a time of unusual geomagnetic behavior with low-amplitude, difficult-to-correlate marine magnetic anomalies. The unique, low-amplitude character of the magnetic anomalies has invoked discussion about the nature of the Jurassic magnetic field. It was once suggested that this Jurassic ''Quiet Zone'' (JQZ) reflects a period during which the geomagnetic field did not reverse, analogous to the Cretaceous Quiet Zone [e.g., *Heirtzler and Hayes*, 1967; *Larson and Pitman*, 1972; *Hayes and Rabinowitz*, 1975; *Barrett and Keen*, 1976]. Contemporaneous land magnetostratigraphic data contain many geomagnetic field reversals [*Steiner*, 1980; *Ogg et al.*, 1984; *Steiner et al.*, 1985; *Steiner et al.*, 1987; *Ogg et al.*, 1991; *Ogg and Gutowski*, 1995], suggesting that the JQZ is instead a period of rapid polarity reversals. Whether the small-amplitude JQZ anomalies represent actual geomagnetic field reversals or intensity fluctuations is a debate with fundamental implications for the interpretation of the geomagnetic polarity reversal timescale (GPTS) and implied reversal rates, which may have been higher than at any time in recorded geomagnetic history [e.g., *Cande and Kent*, 1992a, 1992b; *Sager et al.*, 1998; *Roeser et al.*, 2002; *Bowles et al.*, 2003; *Tivey et al.*, 2006].

[3] The JQZ encompasses middle to Late Jurassic age seafloor in both Pacific and Atlantic oceans where magnetic lineations are reduced in amplitude to the point of incoherence. Over the years, the age of the young edge of the JQZ has been pushed farther back in time as small, correlatable anomalies were recognized deeper in the anomalous zone [e.g., *Larson and Hilde*, 1975; *Cande et al.*, 1978; *Handschumacher et al.*, 1988; *Sager et al.*, 1998]. Although M29 is the oldest anomaly accepted in most GPTS models [*Channell et al.*, 1995], aeromagnetic and deep-tow magnetic data show many older anomalies in the Pacific JQZ [*Handschumacher et al.*, 1988; *Sager et al.*, 1998]. These older anomalies are more apparent in aeromagnetic and deep-tow data because these techniques

[1]Department of Oceanography, Texas A&M University, College Station, Texas, USA.
[2]Department of Geology and Geophysics, Woods Hole Oceanographic Institution, Woods Hole, Massachusetts, USA.
[3]School of Earth and Environmental Science, Seoul National University, Seoul, Korea.

0148-0227/08/2007JB005527$09.00

allow better separation of external geomagnetic field variations relative to crustal anomalies than do ship-towed sea surface magnetic profiles.

[4] A 1992 deep-tow magnetic anomaly survey investigated the western Pacific JQZ in Pigafetta Basin [*Sager et al.*, 1998], where *Handschumacher et al.* [1988] previously mapped pre-M29 anomalies using aeromagnetic data. Pigafetta Basin was also drilled by the Ocean Drilling Program (ODP) during Legs 129 and 185, coring Jurassic basalt in Hole 801C [*Lancelot et al.*, 1990; *Plank et al.*, 2000]. Pigafetta Basin magnetic anomalies provide a high-resolution record because of rapid spreading (~65–79 mm/a half rate) of the ancient Pacific-Izanagi Ridge [*Nakanishi et al.*, 1989; *Sager et al.*, 1998]. The 1992 study was limited by having only two parallel deep-tow profiles, which left the repeatability of the oldest and smallest anomalies in question. Furthermore, the two deep-tow lines do not extend to either Hole 801C or the "rough-smooth boundary" (RSB) that is thought to be the end of the small anomaly sequence [*Handschumacher et al.*, 1988; *Abrams et al.*, 1993].

[5] In this study, we sought to investigate the nature of the JQZ anomalies by collecting new deep-tow data. We tested anomaly repeatability by collecting multiple, closely spaced lines at two locations. We also extended the deep-tow profiles past Hole 801C, southeast to the RSB to provide a record of the complete anomaly sequence. This approach was a compromise because time constraints would not permit a large number of magnetic profiles to be collected over the entire 950-km length study area. In a previous publication [*Tivey et al.*, 2006], we presented a preliminary analysis of these data, including a GPTS. In this study, we present the underlying derivation of that timescale and a more in-depth examination of the anomalies, their correlation, and their implication for the nature of the JQZ geomagnetic field based on both the new data and existing data.

1.1. Geological Background

[6] Pigafetta Basin is located within the Marcus-Wake seamounts in the western Pacific Ocean, 500 to 1000 km east of the northern Marianas Trench (Figure 1). The abyssal seafloor is mostly flat and nearly featureless and has an average depth of 5705 m (1σ = 156 m), with igneous basement below a few hundred meters of abyssal pelagic sediment [*Lancelot et al.*, 1990; *Abrams et al.*, 1993]. The oceanic lithosphere was originally formed at the NE-trending Pacific-Izanagi Ridge during the Jurassic [*Nakanishi et al.*, 1992]. Paleomagnetic studies at ODP Sites 800 and 801 indicate that Pigafetta Basin lithosphere formed slightly south of the equator, then moved northward to its current location [*Larson et al.*, 1992]. The most significant post-Jurassic geologic event that occurred in the basin was intraplate volcanism during the Early and Middle Cretaceous, causing the emplacement of several plateaus, numerous seamounts, and massive sills [*Schlanger et al.*, 1981; *Koppers et al.*, 2003b]. Although such volcanism has the potential to destroy prior magnetic signatures in the oceanic crust, various studies have documented correlatable Jurassic and Early Cretaceous magnetic lineations in this region [e.g., *Larson and Schlanger*, 1981; *Nakanishi et al.*, 1992]. Two factors are thought to explain the survival of pre-Cretaceous anomalies: (1) volcanic source vents were narrow and the sills mainly intruded the sediment column and (2) laterally extensive, uniformly magnetized sills should produce a significant magnetic anomaly only at their edges [*Larson and Schlanger*, 1981].

[7] ODP Legs 129 and 185 succeeded in penetrating ~474 m into Jurassic oceanic crust at Hole 801C [*Lancelot et al.*, 1990; *Plank et al.*, 2000]. Ar^{40}/Ar^{39} geochronology indicates that the oldest Jurassic basement is 167.4 ± 1.7 Ma. This unit is overlain by ~165 m of presumably off-axis lavas with ages of 159.5 ± 2.8 and 160.1 ± 0.6 Ma [*Koppers et al.*, 2003a]. Results of basalt core paleomagnetic and downhole magnetic log measurements from Hole 801C show four zones of alternating polarity in the upper younger extrusive volcanic flows and two zones in the oldest Jurassic aged basement [*Plank et al.*, 2000; *Steiner*, 2001; *Tivey et al.*, 2005].

2. Data and Methods

2.1. New Data Collection

[8] We used deep-tow magnetic data collected in 1992 by R/V *Thomas Washington* (cruise TUNE08WT) [*Sager et al.*, 1998] and in 2002/03 by R/V *Thomas G. Thompson* (cruise TN152). During TUNE08WT, a three-axis deep-tow fluxgate magnetometer was towed ~1000–1500 m above the seafloor at an average speed of 2.1–2.5 kt (1.1–1.3 m/s). During cruise TN152, a three-axis magnetometer was mounted on the deep-tow DSL-120 side-scan sonar and towed ~100 m above the seafloor, controlled by onboard winch to maintain this depth, at an average speed of 1.2 kt (0.56 m/s). Track lines were designed to avoid seamounts and to be oriented nearly perpendicular to the previously mapped magnetic lineations (Figure 1).

[9] The position of the DSL-120 vehicle was calculated from the ship's GPS-determined location using the vehicle layback measured from acoustic slant range between the ship and the DSL-120. The slant range calculation was calibrated during the detailed survey around Hole 801C when a network of four transponders were deployed on the seafloor to determine the deep-tow vehicle position using acoustic triangulation. This calibration step improved the accuracy of the layback calculation using slant-range only for those survey lines outside of the transponder network.

[10] Three closely spaced, subparallel lines (lines 5-11, 5-12, and 5-13) were run over the extrapolated position of anomaly M34, a well-defined anomaly from the 1992 survey (Figures 2 and 3). The rationale for this minisurvey was to examine anomaly repeatability in a part of the JQZ with well-defined, rapidly varying anomalies. Seven subparallel profiles (lines 1, 2-1, 2-3, 2-5, 2-7, 3-4, 3-6, and 3-9) were also collected in a small area around the Hole 801C drill site (Figures 2 and 3). The purpose of this minisurvey was to confirm the existence of lineated magnetic anomalies in the vicinity of Hole 801C and to examine the correlation of these anomalies with the downhole core and downhole logging results (described by *Tivey et al.* [2005]). Two 125-km long subparallel lines were extended from Hole 801C south to the RSB (Lines 1 and 3-9) in order to complete the oldest continuous seafloor record possible in this area. In the northern part of the study area (Figures 1 and 4), a single survey line was extended from the flank of Golden Dragon seamount south to Hole 801C, between the

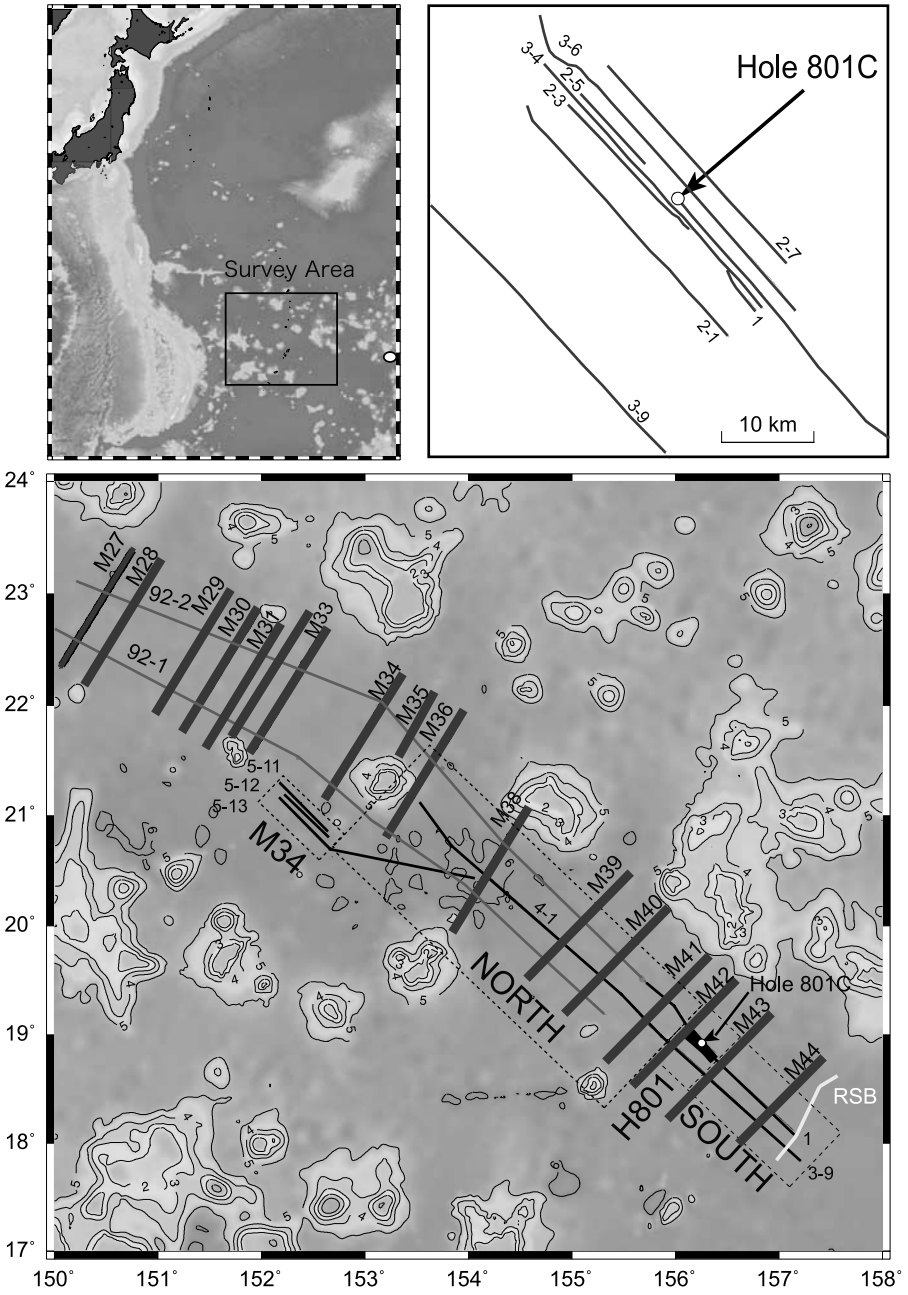

Figure 1. Location of survey area and ship tracks. Bottom chart shows bathymetry map (1000-m contours) with selected magnetic lineations (northeast trending gray lines) and previous deep-tow magnetic profiles (northwest trending gray lines) from *Sager et al.* [1998]. Deep-tow magnetic profiles collected on cruise TN152 for this study are shown by thin black lines and Rough-Smooth Boundary (RSB) by the light line. Dotted boxes show named subsets of the survey. Small numbers are line identifiers. Upper left panel gives location of study area in regional context with land shown dark gray. Wake Island location is shown as open circle. Upper right panel is an enlargement of the survey lines over ODP Hole 801C (open circle).

two profiles from the TUNE08WT cruise (new lines 4-1, 3-9 (contiguous) between old lines 92-1, 92-2). These new data were intended to connect the recent survey data with the previous deep-tow magnetic profiles and to examine anomalies in an area of uncertain correlation. For reference, we refer to the four regional subsets of new survey data as M34, H801, SOUTH, and NORTH (Figure 1).

2.2. Magnetic Data Processing

[11] A total of ~1550 km of new magnetic data from the TN152 cruise were corrected and processed through the following seven steps: (1) calibration of the fluxgate magnetometer output to absolute magnetic field, (2) merging of magnetic data with navigation and attitude data, (3) international geomagnetic reference field (IGRF) correction, (4) external field

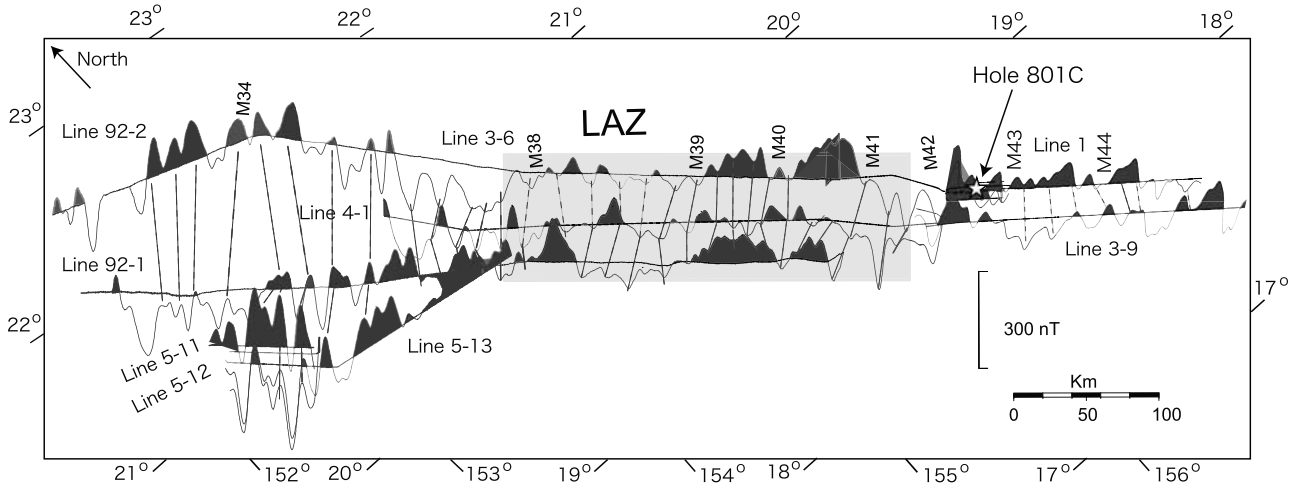

Figure 2. Observed deep-tow magnetic anomaly data plotted perpendicular to ship tracks. Light wiggly lines are magnetic anomaly data with positive anomalies shaded gray. Dashed lines show anomaly correlations. LAZ (gray area) stands for "low-amplitude zone" (see text). Magnetic anomalies in this and subsequent plots are plotted as observed anomalies and have not been deskewed (as in the work of *Sager et al.* [1998]).

variation removal, (5) along-track resampling into equally spaced points, (6) projection onto a common azimuth, and (7) upward continuation from an uneven level to constant depth at several levels using a Fourier transform method [*Guspi*, 1987]. Most of these steps (1, 2, 5, and 6) were to prepare the data for analysis and do nothing to change data character. Step 3, the IGRF correction, is a standard processing step to remove the best available model of the main geomagnetic field. This step yields magnetic anomaly values. For this IGRF correction, we subtracted model field values calculated from IGRF 2000 [*Olsen et al.*, 2000]. Step 4, the removal of short-term external field variations, was done to avoid interpretation of such variations as a crustal field signal. As for step 5, along track resampling was necessary for subsequent Fourier transform calculations that require equally spaced data. This resampling works as a high-cut filter (1 sample/167 data points) on the raw data. Both steps 6 and 7 optimize the magnetic anomalies for qualitative correlations. The upward continuation step acts as a low-pass filter, isolating the longer wavelengths and allowing comparison of the deep-tow data with other magnetic records that were not collected at the ocean floor.

[12] For external field corrections, we used the magnetic variation record from nearly Wake Island (19.17°N, 166.36°E, Figure 1) for most survey days, when such data were continuous and of good quality. For several Wake Island data gaps, we used data from the magnetic observatory at Guam. Guam data were filtered to obtain the long-wavelength diurnal external field variation, scaled for latitude change in daily range (using curves from *Onwumechili* [1967]), and substituted for the missing parts of the Wake Island data. Calculated daily magnetic variations range from ~30 to 80 nT and average 50.4 nT (see Figure S1 in the auxiliary material[1]). Corrected variation data were shifted in time by the difference in solar time between the station at Wake Island or Guam and the ship location, and were subtracted from the total field magnetic measurements. Because the external field variation correction is longer in wavelength and lower in amplitude than most deep-tow anomalies, these corrections made little change in the anomaly sequence character (see Figure S1).

[13] The deep-tow magnetic profiles show such high resolution that it is sometimes difficult to discern long-wavelength anomaly features, making correlation with nearby tracks and sea surface data difficult. To emphasize longer wavelengths, deep-tow data were upward continued to three levels: −5.5 km, −3.0 km, and 0.0 km (sea surface) levels. The −5.5 km level reflects a small amount of upward continuation that removes depth variations of the magnetometer, which followed seafloor topography at 100 m altitude. The middepth (−3.0 km) level and sea surface levels were calculated to enhance longer wavelength anomalies by filtering out shorter wavelengths. Using the upward-continued data allowed us to more easily match longer wavelength (~30 km) anomalies, which sometimes provide a reference to help in correlating smaller anomalies [*Sager et al.*, 1998].

2.3. Magnetic Polarity Block Model

[14] Correlation models were made by matching peaks and troughs of the magnetic profiles using inspection. These correlations were used as the basis of a polarity block model. We constructed the polarity model for two reasons. First, this model gives us a time series that can be analyzed to understand changes in geomagnetic field behavior. Second, when calibrated with absolute age, a polarity block model can be used to derive a GPTS that can be compared with other marine magnetic records or with magnetic stratigraphy on land. Because we do not know which anomalies result from true magnetic reversals and which are caused by other geomagnetic field variations, this model has uncertainty than can only be resolved by comparison with other similar records (see section 4).

[15] Our approach to making a polarity block model was to first use a potential field inverse modeling technique

[1]Auxiliary materials are available in the HTML. doi:10.1029/2007JB005527.

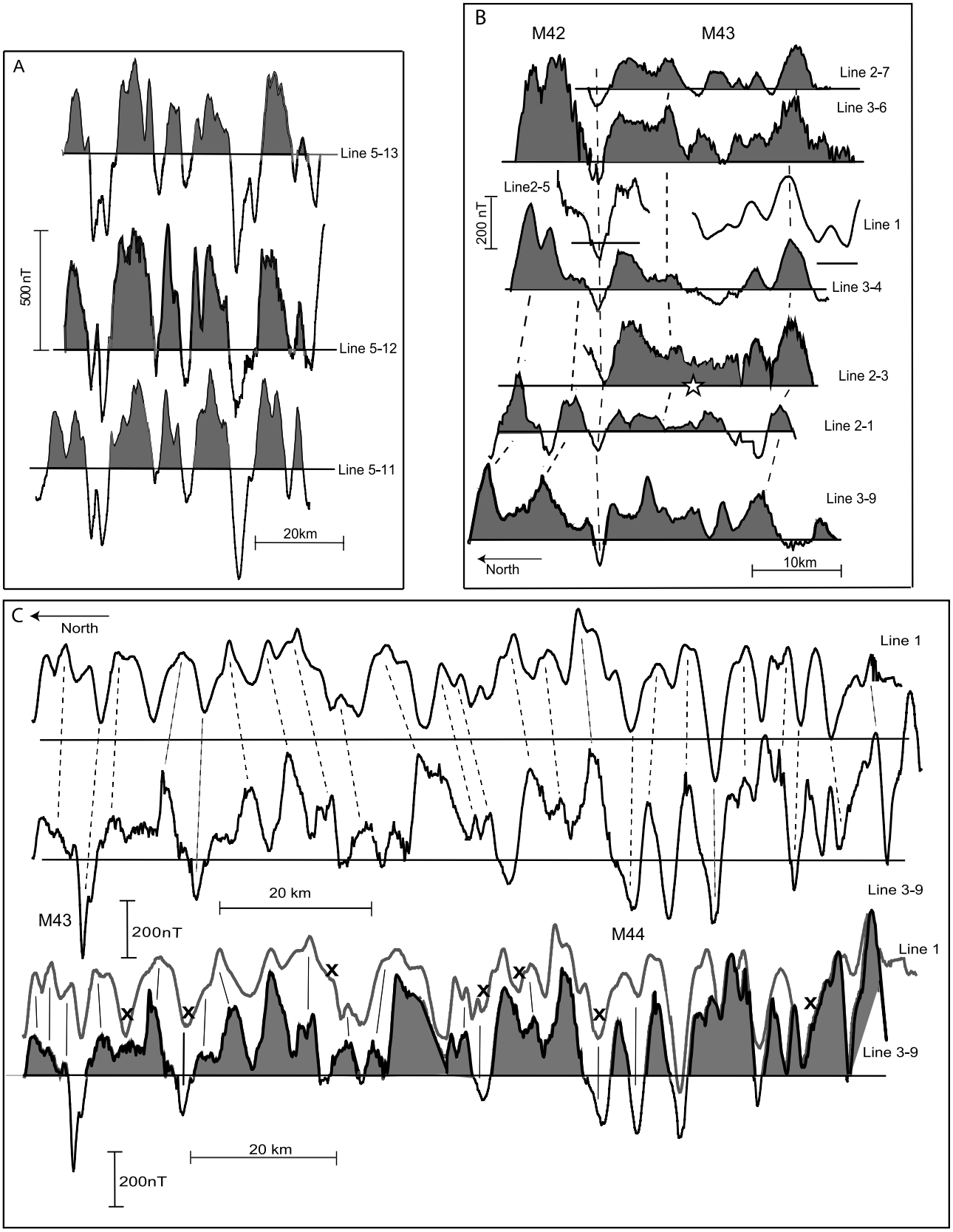
A
Line 5-13
500 nT
Line 5-12
Line 5-11
20km
B
M42
M43
Line 2-7
Line 3-6
Line2-5
200 nT
Line 1
Line 3-4
Line 2-3
Line 2-1
Line 3-9
North
10km
C
North
Line 1
20 km
Line 3-9
M43
200nT
M44
Line 1
Line 3-9
20 km
200nT

Figure 3

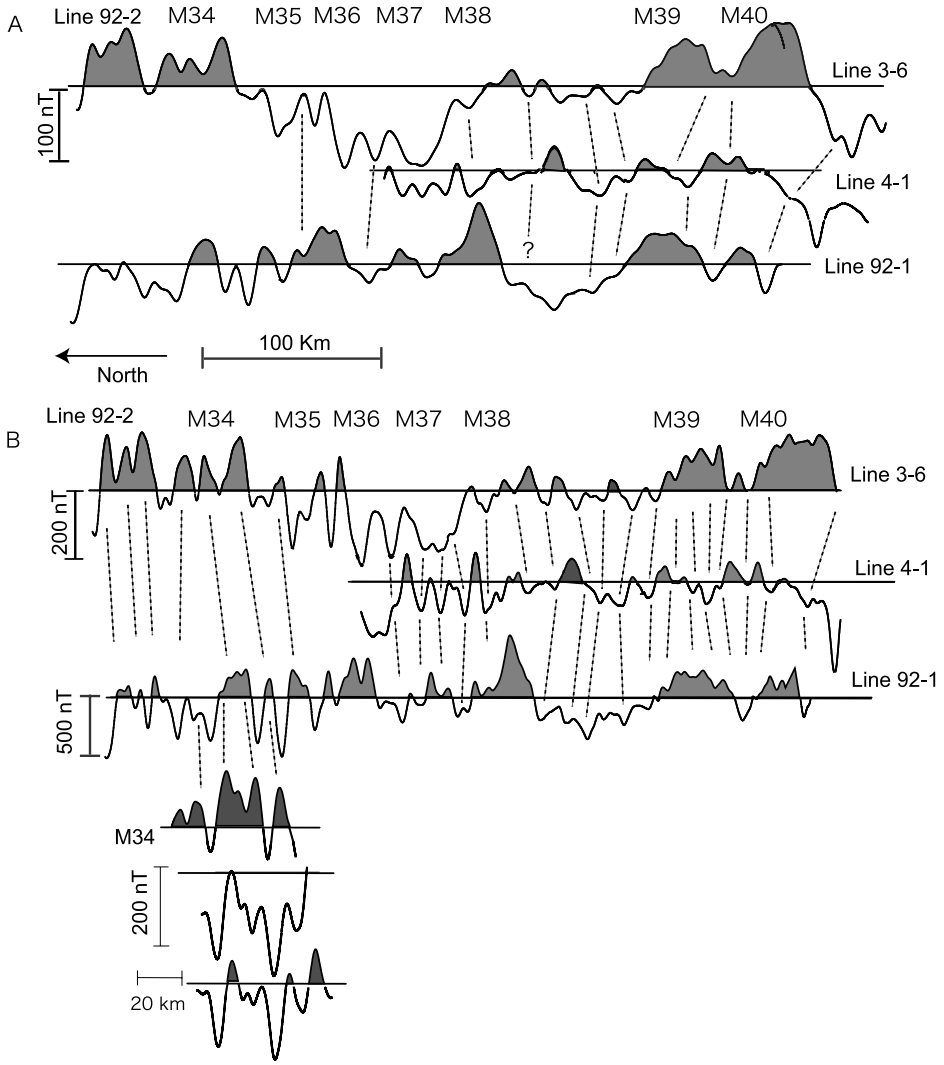

Figure 4. Correlation of deep-tow magnetic profiles in the NORTH survey area, upward continued to (a) sea surface and (b) midwater (−3.0 km). Lines 92-1 and 92-2 are from *Sager et al.* [1998] (note that uppermost line is mostly line 92-2 with a small segment, line 3-6, added from recent survey). These older data are not shown deskewed as in some plots from *Sager et al.* [1998]. Plot shading and annotation conventions as in Figure 3. Locations shown in Figures 1 and 2.

[*Parker and Huestis*, 1974] to make a preliminary interpretation of magnetization and to refine the fit of observed and modeled anomalies with forward modeling [*Parker*, 1972] (see description in Figure S2). *Cande and Kent* [1992a] used zero-crossings of deskewed anomalies (similar to our inverse magnetization model) to determine polarity boundaries; however, because the JQZ magnetic anomalies have low amplitude, it is difficult to determine polarity boundaries solely by zero-crossings. Long wavelength magnetic variations and the adjustment of the local annihilator function (which we set to zero under the assumption of equal normal and reversed polarity crust) can both affect zero crossings for the small JQZ anomalies, so we used zero-crossings only for a first approximation of polarity boundary locations.

[16] For both inverse and forward models, we filtered out long (>140 km) and short wavelengths (<3 km) to focus on the medium wavelength magnetic anomaly character. Models used an ambient field inclination of 23° and declination of 3°, calculated from the IGRF at latitude and longitude of

Figure 3. Correlation of deep-tow magnetic profiles in the (a) M34, (b) H801, and (c) SOUTH survey areas. Gray filled anomaly curves indicate positive observed anomalies whereas black horizontal lines denote zero value. Dashed lines show correlations. Survey subarea locations are shown in Figures 1 and 2. In Figure 3b, star shows location of Hole 801C. Lines 1 and 2-5 are nearly coincident with Line 3-4 and are not shaded in plot. In Figure 3c, plot shows improvement in anomaly correlation with modest (<5 km) stretching and shrinking of parts of Line 1 to fit peak and trough spacing on Line 3-9. The cross symbols show tie points used for adjustment.

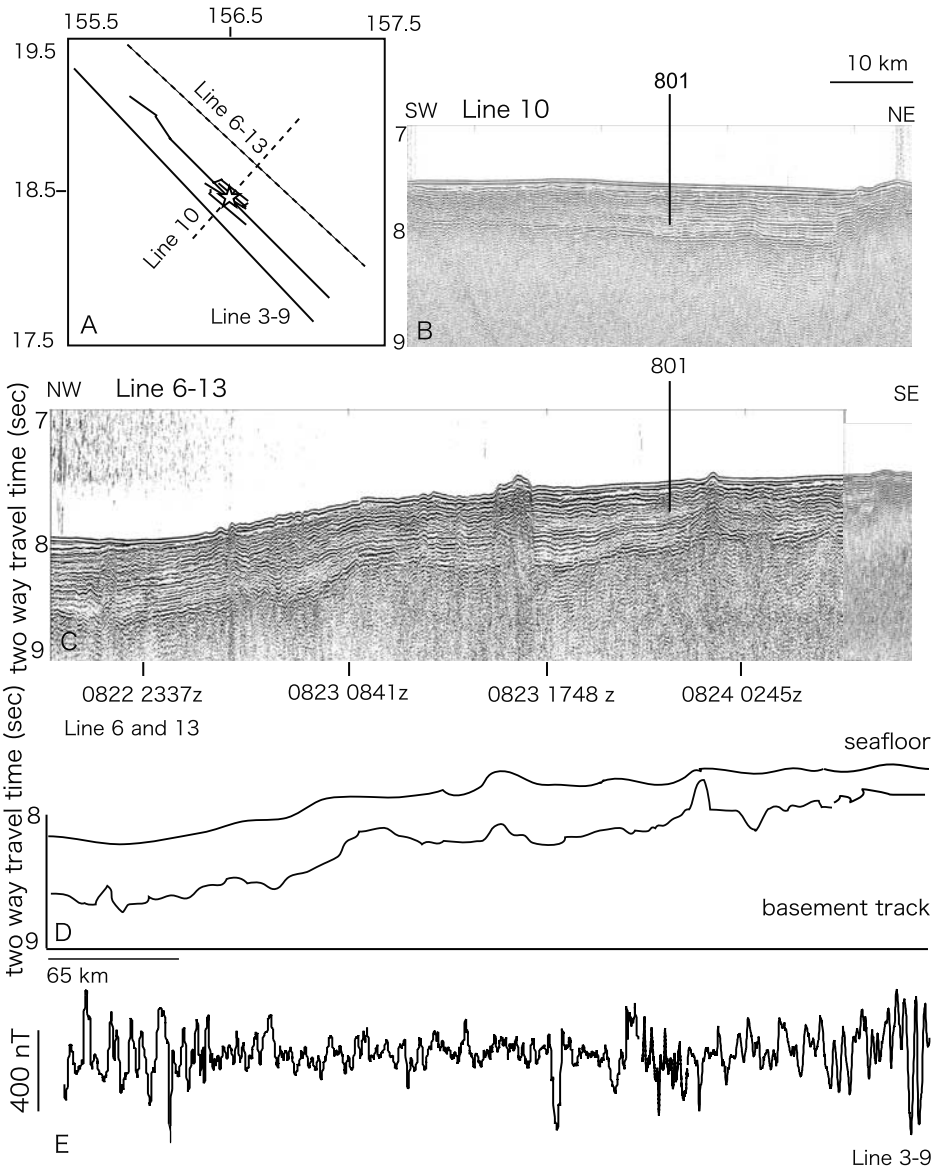

Figure 5. Plot of seismic profile and deep-tow magnetic data. (a) Spatial relationship of seismic lines from MESOPAC II [*Lancelot*, 1989] and survey lines from this study. Solid lines show magnetic survey line in this study and dotted lines are lines 6-13 and 10 from MESOPAC II. (b) Line 10 seismic data from MESOPAC II. Vertical line indicates the location of Hole 801 C. (c) Line 6-13 seismic data from MESOPAC II. (d) Seafloor and oceanic basement interpreted from data shown in Figure 5c. (e) −5.5 km level Line 3-9 magnetic line from this study shows that magnetic anomalies are not correlated to basement topography.

Hole 801C. We used a paleofield inclination and declination of −10° and 20°, respectively (from *Larson and Sager* [1992]) and defined the strike of the magnetic anomalies as 135° clockwise from north (from *Sager et al.* [1998]). Although *Tivey et al.* [2006] suggested that there may be slight directional changes in anomaly strikes, we kept this constant strike because the strike changes are uncertain and this assumption is consistent with previous studies [*Handschumacher et al.*, 1988; *Sager et al.*, 1998] (also see sections 3.1, 4.1, and 4.4). Magnetic models require appropriate values for the seafloor depth, sediment thickness, and thickness of the magnetic source layer. While seafloor depth is available from the DSL-120 side-scan sonar data, the depth of igneous basement must be interpreted from sparse, pre-existing seismic profiles [*Abrams et al.*, 1993] and the Hole 801C. We were unable to obtain seismic data along the deep-tow profiles during the TN152 cruise because of time and logistical limitations. For simplicity in modeling, we used a constant depth for the seafloor and sediment thickness within each survey subarea: −5.6 and −6.1 km (seafloor and basement) for the M34 survey, −5.6 and −6.2 km for the NORTH survey, −5.5 and −5.9 km for the H801C survey, and −5.6 and −6.1 km for the SOUTH survey. As shown in Figure 5, changes in seafloor depth and sediment thickness are mostly gentle, so these approximations should be reasonable. For reference,

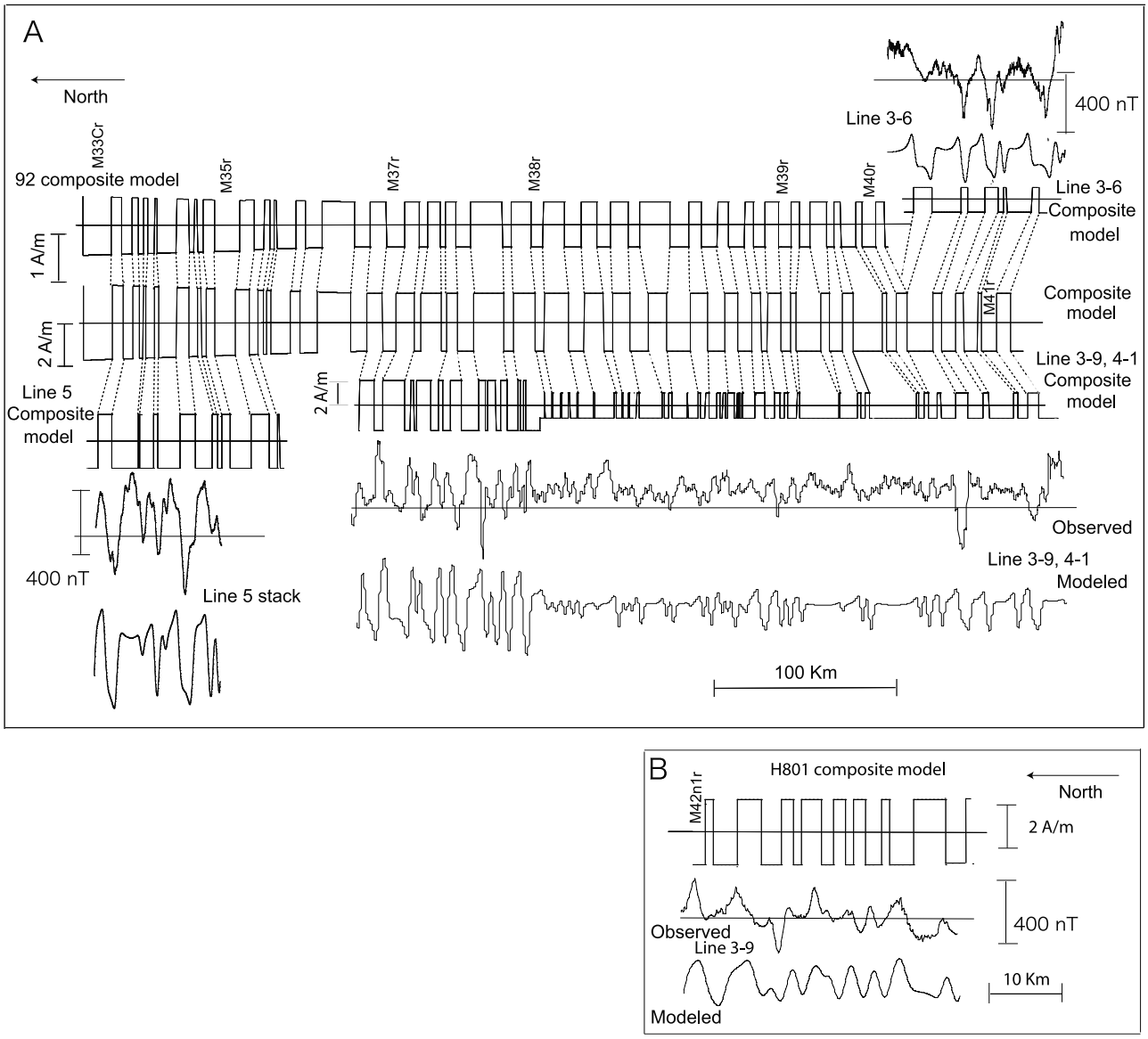

Figure 6. Polarity block models. Square-wave profiles represent magnetization for polarity block models with positive magnetization (above zero lines) representing normal polarity and negative, reversed polarity. Dotted lines show correlations. Solid lines show deep-tow magnetic anomaly data. (a) Polarity block model for the NORTH survey area. Model "92 composite" at top is from *Sager et al.* [1998]. Line 3-6, 5, and 3-9, 4-1 models are from this study. "Composite model" at center is a combination of all polarity block models. (b) Polarity block model for the H801 survey area. The polarity model was derived from a stack of nine anomaly profiles; line 3-9 is shown here as an example compared with the predicted model field. (c) Polarity block model for the SOUTH survey area Top profiles show the observed (bold) and predicted anomalies for line-1. Bottom profiles show observed (bold) and modeled anomalies for line 3-9. Center square wave plots show polarity model correlations and final "combined" model. Plot conventions as in previous figures.

the sediment thickness drilled at Hole 801C was approximately 463 m [*Plank et al.*, 2000].

[17] Although there is no constraint for the thickness of the magnetic source layer, most marine magnetic models assume that the crustal extrusive lavas are the primary source and have thicknesses of 500 to 1000 m. The extrusive layer in Hole 801C is at least 474 m thick [*Plank et al.*, 2000], but since we do not know how much of that layer extends below the bottom of the hole, we chose 1000 m as the nominal source layer thickness for modeling. This choice for source layer thickness is not likely to have a significant effect on the interpretation of modeled polarity sequence.

[18] After a preliminary polarity model was derived from the inverse calculations, this model was used as the input magnetization distribution for subsequent forward modeling. In the forward model, magnetization strength was estimated from the standard deviation of the absolute values

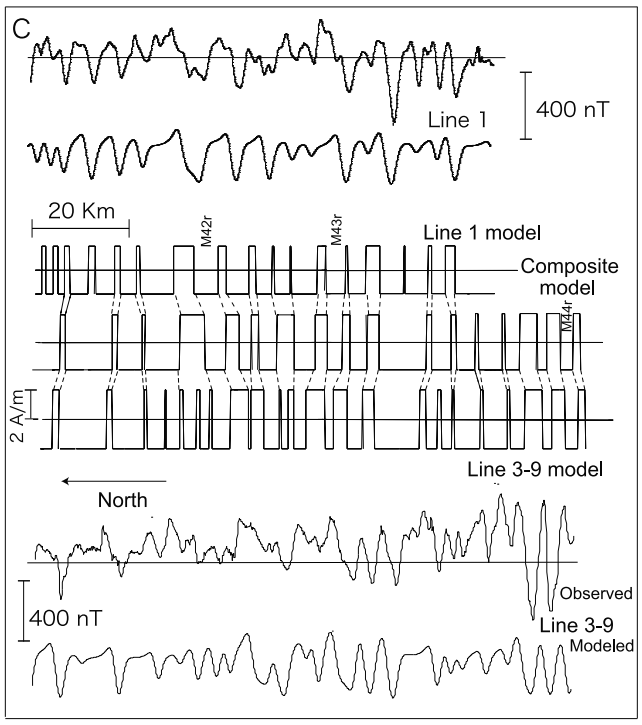

Figure 6. (continued)

of magnetization values calculated by inverse modeling. Although *Sager et al.* [1998] applied an exponential reduction in the magnetization strength with an initial magnetization of 2.25 Am^{-1}, we did not find this model to be an especially good approximation for the new data. For our analysis, anomaly amplitudes were adequately approximated with a constant magnetization in each of the study areas. The magnetization values used in this study are as follows: 3.9 Am^{-1} for M34, 1.7 Am^{-1} for H801C, 2.0 Am^{-1} for NORTH, and 2.3 Am^{-1} for SOUTH. These values provide the best match in terms of amplitude and shape between observed and calculated magnetic anomalies. The magnetizations for H801C, NORTH, and SOUTH are essentially the same. The M34 survey magnetization is nearly twice as high because the magnetic anomalies in that area have significantly larger amplitudes (Figures 2 and 3). A Gaussian filter (σ = 7 km) was applied to the forward models to give finite-width reversal transitions, which give a better fit of observed and modeled anomaly slopes [*Schouten and Denham*, 1979].

2.4. Composite Model

[19] Once magnetic polarity block models were constructed for each survey line, a composite model was compiled from the overlapping lines (Figures 6 and 7. The purpose was to create a reversal sequence common to all lines within a given survey area. From the *Sager et al.* [1998] study, we adopted the composite model for the two previous deep-tow lines (92-1 and 92-2) as a starting point for the NORTH area where new and old data overlap. The boundary locations of each polarity block in the composite model were calculated by averaging values of corresponding block boundary distances. In the case of two or more polarity blocks on one line corresponding to only one block on another line, the multiple blocks were merged and modeled as one polarity period in the composite model. This procedure minimizes the number of modeled polarity blocks.

2.5. Age Calibration

[20] Mesozoic magnetic anomalies have only a few good absolute age calibration points with which to interpolate or extrapolate the ages of chron boundaries. *Sager et al.* [1998] used the radiometric date of M26r (155.3 ± 3.4 Ma) from the Argo Abyssal plain [*Ludden*, 1992] to tie the 1992 deep-tow lines to that anomaly in Pigafetta Basin. They extrapolated the ages of blocks from M25 backward in time using the existing GPTS at the time [e.g., *Gradstein et al.*, 1995; *Handschumacher et al.*, 1988]. Our approach was to use the absolute age for M26r and a new high-precision age determination for the tholeiitic basalt layer in Hole 801C (167.4 ± 1.7 Ma) [*Koppers et al.*, 2003a] as tie points on both ends of the survey lines, with linear interpolation in between, assuming a constant spreading rate. The interpolation used the following age-distance relation:

$$\text{Age(Ma)} = 0.0146 \times \text{distance(km)} + 155.3\text{Ma},$$

corresponding to a half spreading rate of 67 km/Ma (Figure S3). To make an age model for anomalies older and younger than the calibration points, we extrapolated this relation, using the polarity block model of *Sager et al.* [1998] for younger anomalies.

[21] Error estimates for the two radiometric dates contribute an uncertainty in the modeled spreading rate. The minimum and maximum slopes that fit the 1-sigma uncertainty bounds on the radiometric ages are 51 km/Ma and 98 km/Ma. Although such extreme slopes are possible given the calibration point uncertainties, the highest and lowest implied values are unlikely because they quickly produce unreasonable ages when extrapolated outside the local survey region.

3. Results

3.1. Anomaly Correlation

[22] What is "good" correlation? Naturally, this is subjective and what is considered good or acceptable correlation varies among analysts. To provide a quantitative foundation, we computed coherency (cross-correlation) among many of the deep-tow profiles and a comparison with established correlated sea surface anomalies (Figure 8). With "good" correlation, anomalies on adjacent profiles have similar shape and spacing. Such profiles have low-lag coherency values typically above ~0.6 (e.g., GH824A versus GH7901 in Figure 8). Profiles with anomalies that show dissimilarities in anomaly size and shape (e.g., GH824B versus GH7901 in Figure 8), typically have low-lag coherency values of less than 0.4. In our study area, the between-line correlation of the deep-tow anomalies in our study is mostly excellent to good in all areas except for the NORTH area. The best correlation was in the M34 survey where anomalies were closely matched on adjacent lines (Figure 3). In the M34 survey, anomaly amplitudes are relatively large (~500 nT) and the anomalies show only small differences in anomaly shape and size between lines.

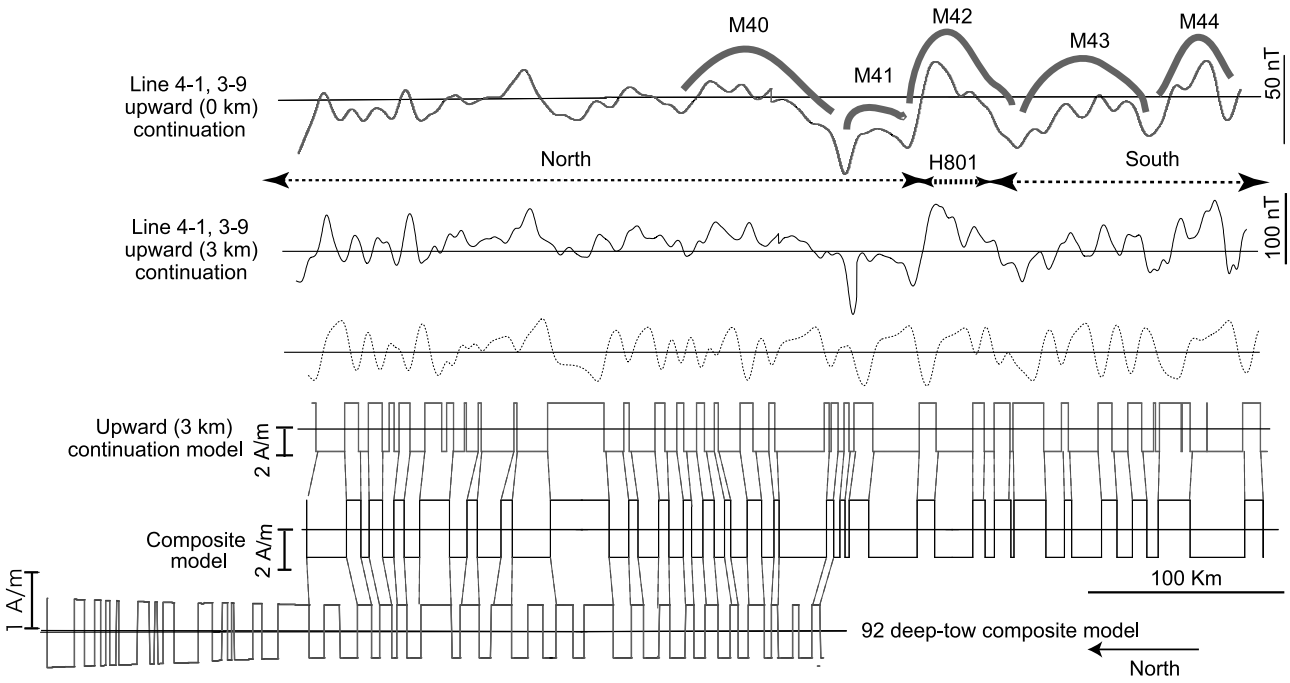

Figure 7. Polarity block model for entire survey, shown for midwater depth (−3.0 km). Magnetic anomalies have not been deskewed. Top two solid curves show observed magnetic anomalies at sea surface (0 km) and 3 km depth. Dotted curve shows calculated magnetic anomalies. Bottom square wave plots show final combination model based on reconciling the 92 model and the new data.

Correlation functions between lines are >0.5 at low offset (Figure 8), indicating a high level of agreement. The worst correlation was in the NORTH survey area, which contains small, difficult-to-correlate anomalies as we had found previously in the 1992 survey (Figure 4).

[23] Profiles in the H801 survey, where anomaly amplitudes are mostly <200 nT at the deep-tow level, also show good correlation by eye (Figure 3). In comparison with the M34 profiles, these anomalies show greater variability in size, position, and shape, but because we have so many closely spaced lines, the correlation is convincing. The correlation function is >0.5 for lines 2-7 and 2-3, which are ∼10 km apart, but never >0.2 for lines 2-7 and 3-9, which are ∼30 km apart (Figures 3, 8). The reasons for the poor correlation are apparent from an inspection of the two profiles (Figure 3); these are probably the most dissimilar lines in terms of anomaly spacing and amplitude. Nevertheless, these two profiles exhibit obvious similarities. For example, for line 3-9 the two main anomalies allowing correlation are the deep low on the north center end of the line (∼13 km from north end) and the large, double-positive anomaly on the south end (∼10 km from south end) (Figure 3). In most studies of magnetic anomalies, this degree of correlation would be considered acceptable. Because of the anomaly variations, correlation in the H801 area would be less convincing if only two or three widely spaced profiles were available, a factor to be considered when we interpret other areas of JQZ data.

[24] Anomalies in the SOUTH survey have amplitudes of ∼200 nT (Figure 3). Although we have only two lines (lines 1 and 3-9) located ∼30 km apart, they display generally good agreement between the large anomaly shapes and locations, albeit with some variation in small features, spacing, and amplitude (Figure 3). The correlation coefficient for these two lines peaks at just under 0.5, but can be increased to >0.6 with small (<5 km) adjustments to the spacing of anomalies on line 1 to better match the spacing on line 3-9 (Figures 3 and 8). Such adjustments imply irregularities in the crustal recording of anomalies.

[25] The NORTH survey was the most difficult region to correlate because it contains both large and small amplitude anomalies that are hard to match uniquely among the few available lines (Figures 2 and 4). North of ∼21°N (M34), the anomalies are ∼200 to 300 nT in amplitude and can be correlated well between lines [*Handschumacher et al.*, 1988; *Sager et al.*, 1998]. In contrast, the anomaly sequence extending from just south of 21°N to the northern edge of the H801 survey shows inconsistent anomaly shapes and spacing that makes unequivocal correlations difficult (Figure 4). The area of difficult correlation corresponds to anomalies M36 to M41 from *Sager et al.* [1998] and includes the zone of weakest anomalies, from 21° to 18.5°N, which we have termed the low amplitude zone (LAZ; Figure 2) because of its distinctive subdued anomaly amplitude [*Tivey et al.*, 2006]. In the area northwest of where our profiles intersect 21°N (M36 in Figure 1), the aeromagnetic anomalies in the work of *Handschmacher et al.* [1988] show good correlation across the whole series of profiles. To the southeast of this point, the anomalies are much smaller and more irregular from one profile to the next (see Figures 7 and 11 in that article). This is the area of the LAZ, in which we find correlation difficult, even with the deep-tow profiles. Although the smaller separation of source and sensor enhances the anomaly amplitudes, the repeatability of anomaly signatures from one line to the next is poor.

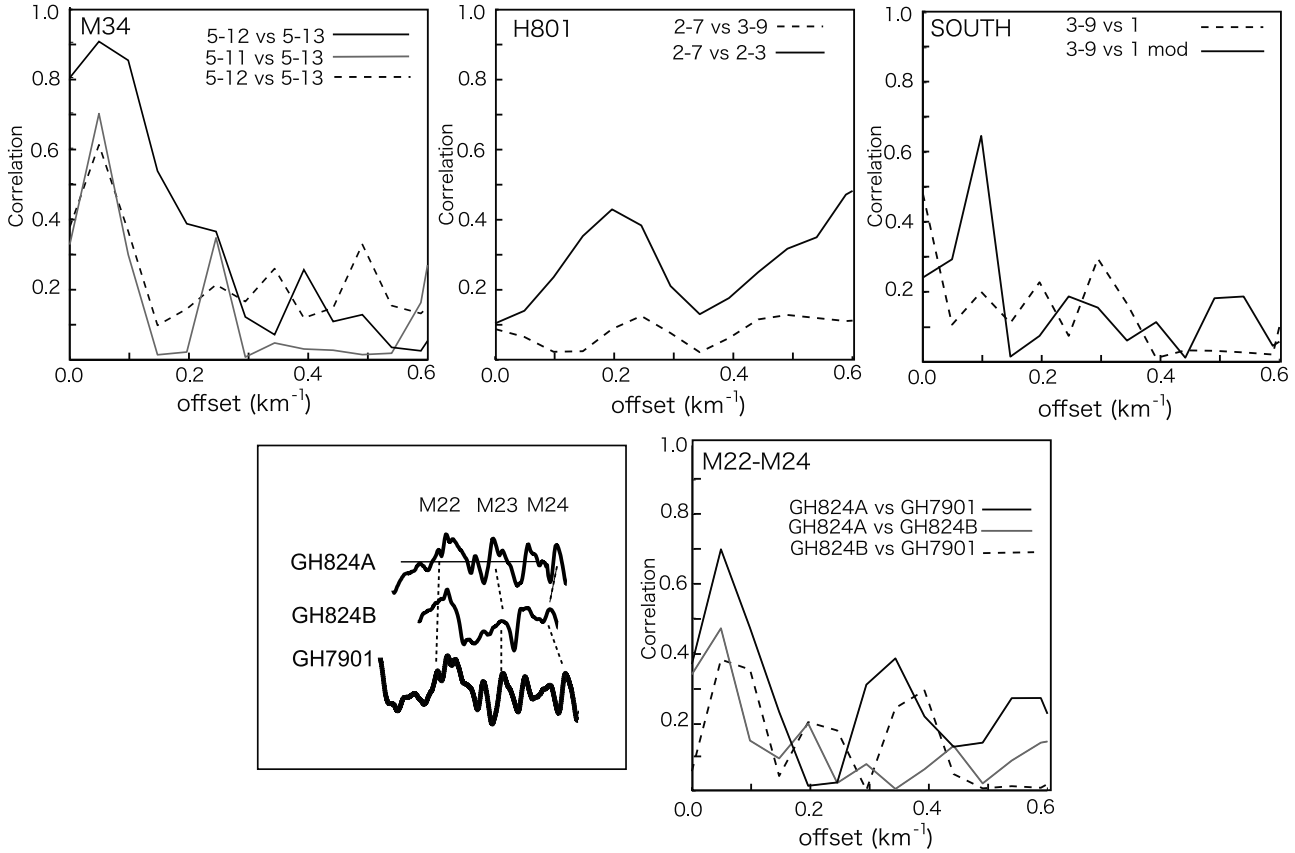

Figure 8. Cross-correlation functions of selected magnetic profiles. Cross-correlation between deep-tow profiles shown in upper row of boxes: (left) lines 5-11, −12, −13 in the M34 area; (middle) lines 2-3, −7, and 3-9 in the H801 area; and (right) lines 1 and 3-9 in the SOUTH area. In the latter plot, the solid line shows the improved coherency attained with modified spacing of anomalies on line 1 (see text and Figure 3). Cross-correlation was not plotted for NORTH area lines because the correlation function is small (<0.2). Lower left box shows for comparison representative M22-M24 surface-towed magnetic anomaly profiles in the Japanese lineations near the Ogasawara Plateau and their well accepted correlations (dotted lines). Lower right box shows cross-correlations for those profiles, for comparison with panels above.

[26] Although our cruise collected one new deep-tow line in the LAZ region, the new data do not improve correlation with the old lines because the shape and amplitude of anomalies on the new line are often different from those on the old lines. Especially confounding are long wavelength (tens of kilometers) anomalies that appear different on the three lines. *Sager et al.* [1998] made a correlation of small anomalies based on the matching of long-wavelength anomalies, which appear similar on the two older profiles, but do not correlate well with the new profile in between. We have mainly followed the previous correlation of smaller anomalies, making a few adjustments as indicated by the new data. Although the degree of correlation is similar to that deemed adequate in other published studies of difficult magnetic lineations [e.g., *Roeser et al.*, 2002], the dissimilarity among large anomalies and the small amplitudes and lack of distinctive character of small anomalies leaves uncertainty in the correlations.

3.2. Polarity Block Model

[27] The polarity blocks modeled for the M34 survey are consistent with coeval anomalies in the study of *Sager et al.* [1998] (Figure 6), so we left this part of the polarity model unchanged. Polarity block models for the H801 and SOUTH areas were developed from the new TN152 data. Because we model high-resolution deep-tow data, both areas show many small-width (short duration) blocks. The composite model for H801, which was stacked from seven profiles (Figure 6), shows a total of 16 reversals over a ~40 km distance. In the SOUTH survey, the composite model derived from the two correlated profiles has a total of 34 reversals in 120 km (Figure 6).

[28] Construction of a polarity block model in the NORTH area was complicated by poor correlations and a difference in resolution between the TN152 and older deep-tow profile data (Figure 6). Essentially, our polarity block model in the NORTH area is the same as that of *Sager et al.* [1998] for the following reasons. The TN152 data were collected significantly closer (1 to 1.5 km) to the seafloor than the previous study, so the new deep-tow data show smaller, shorter wavelength anomalies. As a result, the deep-tow polarity block model for the TN152 profile (lines 3-9 and 4-1) has more polarity blocks, especially in the LAZ

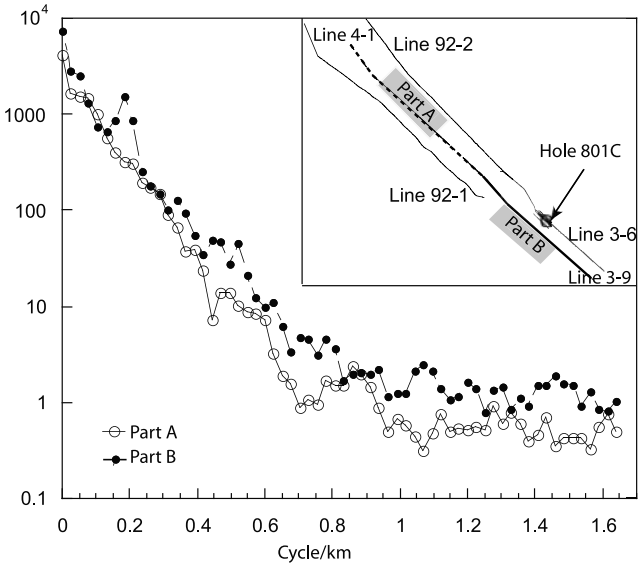

Figure 9. Power spectra for two segments of deep-tow magnetic line 4-1. Vertical axis (logarithmic) plots power spectral density and horizontal axis is frequency. Locations of line segments are shown in the inset. Part A is from LAZ region whereas Part B is from H801 survey. Arrows show break-points on Part A and B spectra.

(Figure 6), than the previous deep-tow model. Because of the method we used to construct the composite polarity block model (i.e., using the minimum number of correlated blocks), this mismatch meant that many of the smaller blocks from the new profile were omitted from the composite polarity model. To assist in correlating blocks in this difficult area, we also constructed and correlated polarity block models using upward continued profiles at −3.0 and 0.0 km. The middle depth model (−3.0 km) compared best with the model of *Sager et al.* [1998] (Figure 7) because its resolution was similar to the shallower deep-tow magnetic profiles collected during the earlier cruise. Although the TN152 deep-tow model implies as many as ∼40 reversals in 100 km, the final composite model retains only about one third as many. We think it likely that some of these short-wavelength anomalies are a result of geologic "noise" (e.g., crustal tectonic emplacement processes, short-period external field fluctuations, or data collection artifacts).

[29] To consider the contribution of geologic noise, we calculated power spectra [*Spector and Grant*, 1970; *Nwogbo*, 1998] for two segments of TN152 lines 4-1 and 3-9, one corresponding to the LAZ and the other from the vicinity of H801 (Figure 9). We expected to see differences in the spectra because of the apparent difference in dominant anomaly wavelengths (Figure 10). A plot of power spectral density shows two approximately linear sections with a break in slope at 0.9 cycle/km for the H801 section and 0.7 cycle/km for the LAZ section. The almost-flat, high-wave number (short-wavelength) section in each spectra is usually interpreted as a noise component [e.g., *Parker*, 1997]. This observation suggests that there is no coherent geologic information at wave numbers >0.7–0.9 cycle/km. Consequently, polarity blocks smaller than 1.2 km (corresponding to wave number 0.8) were dropped from the polarity model.

3.3. Polarity Reversal Models

[30] We constructed two Jurassic GPTS models (Tables 1–2, Figure 11) following the rationale of *Sager et al.* [1998] by producing one at deep-tow depth (−5.5 km) and one at midwater depth (−3 km). In assigning chron numbers to our polarity block model, we numbered anomalies using the upward-continued, sea level data to be compatible with previous GPTS studies that used sea level data (Figures 7 and 11) [*Handschumacher et al.*, 1988; *Cande and Kent*, 1992a; *Sager et al.*, 1998]. The model derived from the −5.5 km depth data assumes that most of the small anomalies (>1.2 km in width) in the deep-tow profiles result from polarity reversals. This gives a large number of polarity chrons and is likely an overestimate of the actual number of reversal periods. The GPTS model constructed from midwater depth profiles may underestimate the number of polarity reversals, but because it is approximately 3 km above the source layer, it is comparable to other GPTS models constructed from magnetic profiles over younger oceanic lithosphere. We did not apply a 30 ka cutoff for cryptochrons, as did *Cande and Kent* [1992a], because this duration is somewhat arbitrary.

[31] Although both deep-tow and midwater GPTS models (Tables 1 and 2) include polarity durations shorter than 30 ka, these short duration chrons only represent 12.5% and 3% of the total number of polarity blocks, respectively. The deep-tow model of the LAZ and H801 areas shows somewhat shorter polarity periods than the midwater model, with

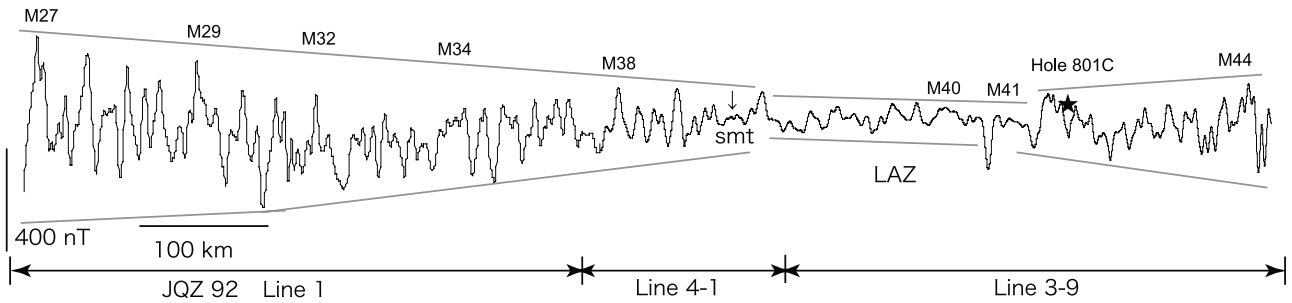

Figure 10. Composite anomaly profile at 4.5 km depth anomalies over the Pigafetta JQZ showing change in anomaly amplitude with age. This composite was constructed from Line 1 of *Sager et al.* [1998] and Lines 4-1 and 3-9 from the subsequent survey. The abbreviation "smt" denotes an anomaly caused by a small seamount. Hole 801C location is shown by star symbol.

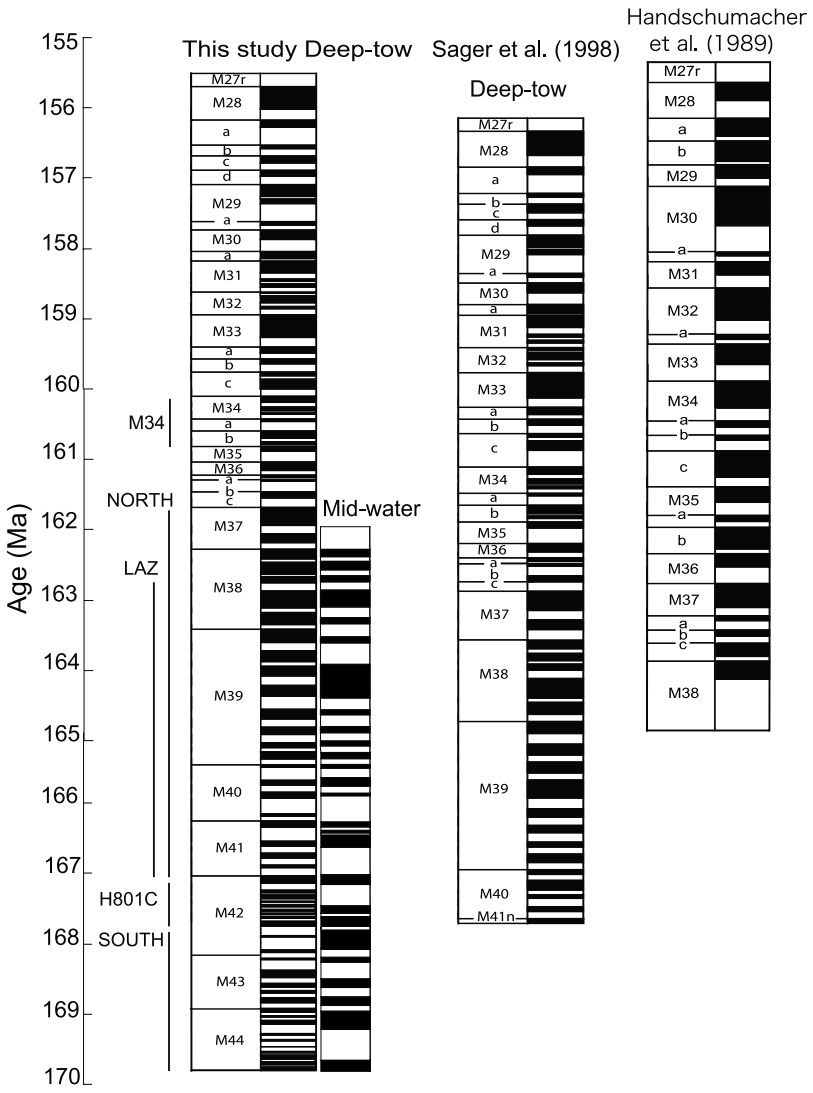

Figure 11. Geomagnetic polarity timescales for the Pacific JQZ derived in this study (left) and prior studies. Left column shows polarity models constructed in this study. That on the left was modeled from deep-tow data, whereas that on the right was modeled from midwater depth profiles. Middle and right columns show polarity models from prior studies. In all columns, black denotes normal polarity and white is reversed polarity. Polarity chrons are listed in Tables 1 and 2.

durations between 14 to 233 ka (average 99 ka). In these areas, approximately 15% of the modeled polarity chrons have <30 ka duration.

[32] In some places, the modeled polarity bias seems to shift between deep-tow and midwater model, particularly around Hole 801C. While the deep-tow model of this area seems to show mostly normal polarity, the upward continued model seems predominantly reverse polarity (Figure 11). This difference is primarily an artifact of the survey sampling and the modeling procedure. Around Site 801, we have many closely spaced magnetic profiles, so the composite polarity model is robust and retains many reversals. Furthermore, between the deep-tow and midwater levels, the modeling shifts from matching the smallest to longer wavelength anomalies. At deep-tow level, the short wavelength anomalies are prominent, but with upward continuation, they disappear or merge into longer wavelength anomalies. Because of the combination of long and short wavelength anomalies on the JQZ magnetic profiles, the result of modeling one versus the other does not always give the same polarity sequence. We believe that this is likely to be a problem in other areas where the magnetic signal contains geologic noise and is not unique to the Pigafetta Basin.

[33] The deep-tow GPTS model (Table 1) also contains artifacts arising from the way in which the correlation model was constructed. The LAZ, which we interpret as having the highest-frequency but lowest-amplitude magnetic anomalies, corresponds to a lesser number of polarity blocks (M38-41) than some other places in the GPTS model, for example, the section over Hole 801C (Figure 11). This apparent discrepancy results from the fact that anomaly correlations were poor in the LAZ, so the polarity model in that zone is mostly based on the older, lower-resolution deep-tow magnetic data and the number of polarity blocks is suppressed by our minimalist correlation procedure. The

Table 1. Deep-Tow Geomagnetic Polarity Reversal Timescale Model

	Distance (km)		Age (Ma)	
Chron	Young	Old	Young	Old
M27r	14.0	25.8	155.5	155.7
M28r	47.3	58.0	156.0	156.2
M28Ar	65.1	81.9	156.3	156.5
M28Br	85.5	91.8	156.6	156.7
M28Cr	99.4	105.9	156.8	156.9
M28Dr	111.6	119.5	157.0	157.1
M29n.1r	130.6	132.8	157.2	157.3
M29r	137.5	154.4	157.3	157.6
M29Ar	157.9	162.6	157.7	157.7
M30r	171.5	183.0	157.9	158.0
M30Ar	190.1	192.4	158.1	158.2
M31n1r	203.5	209.4	158.3	158.4
M31n2r	211.4	214.4	158.4	158.5
M31r	217.5	221.4	158.5	158.6
M32n1r	223.0	225.1	158.6	158.7
M32n2r	232.1	235.9	158.8	158.8
M32r	238.0	244.0	158.8	158.9
M33r	265.3	274.8	159.3	159.4
M33Ar	280.4	285.4	159.5	159.6
M33Br	290.3	298.4	159.6	159.7
M33Cn1r	301.1	304.9	159.8	159.8
M33Cr	313.6	328.3	159.9	160.2
M34n1r	333.9	339.1	160.3	160.4
M34n2r	342.3	344.4	160.4	160.4
M34n3r	345.9	349.9	160.5	160.5
M34Ar	352.3	361.6	160.5	160.7
M34Bn1r	368.1	372.5	160.8	160.9
M34Br	374.5	376.8	160.9	160.9
M35r	381.5	391.9	160.9	161.1
M36n1r	399.4	403.4	161.3	161.3
M36Ar	406.5	407.9	161.4	161.4
M36Br	410.1	420.2	161.4	161.6
M36Cr	425.2	434.1	161.6	161.8
M37n1r	451.5	459.7	162.0	162.2
M37r	467.7	474.6	162.3	162.4
M38n1r	484.0	487.5	162.5	162.6
M38n2r	498.0	500.9	162.7	162.8
M38n3r	506.5	514.5	162.8	162.9
M38n4r	530.3	535.2	163.2	163.3
M38r	546.3	551.0	163.4	163.5
M39n1r	563.4	571.5	163.7	163.8
M39n2r	581.6	586.3	163.9	164.0
M39n3r	595.3	604.4	164.2	164.3
M39n4r	614.8	626.9	164.5	164.6
M39n5r	635.6	644.5	164.8	164.9
M39n6r	651.3	658.5	165.0	165.1
M39n7r	663.3	666.5	165.2	165.2
M39r	673.4	678.7	165.3	165.4
M40n1r	681.5	694.1	165.5	165.6
M40n2r	698.8	705.1	165.7	165.8
M40n3r	709.7	725.7	165.9	166.1
M40r	727.9	732.8	166.1	166.2
M41n1r	738.5	751.6	166.3	166.5
M41n2r	756.2	763.5	166.6	166.7
M41n3r	767.7	774.9	166.7	166.8
M41r	776.8	784.5	166.9	166.9
M42n1r	791.8	799.2	167.1	167.2
M42n2r	800.7	803.7	167.2	167.3
M42n3r	807.2	809.9	167.3	167.4
M42n4r	811.6	812.8	167.4	167.4
M42n5r	815.6	817.2	167.5	167.5
M42n6r	818.9	819.9	167.5	167.5
M42n7r	821.9	823.6	167.5	167.6
M42n8r	825.2	828.1	167.6	167.6
M42n9r	832.8	841.5	167.7	167.8
M42n10r	843.1	855.9	167.9	168.1
M42r	857.6	864.1	168.1	168.2
M43n1r	865.2	874.4	168.2	168.3
M43n2r	881.4	887.1	168.4	168.5
M43n3r	890.8	894.0	168.6	168.6
M43n4r	896.3	901.1	168.7	168.7
M43r	906.0	911.6	168.8	168.9
M44n1r	915.0	918.0	168.9	168.9
M44n2r	919.7	923.2	169.0	169.1
M44n3r	925.7	935.3	169.1	169.2
M44n4r	936.5	940.4	169.3	169.3
M44n5r	941.6	946.8	169.3	169.4
M44n6r	947.6	952.4	169.4	169.5
M44n7r	953.1	956.0	169.5	169.5
M44n8r	959.8	961.6	169.6	169.6
M44r	964.4	967.0	169.7	169.7
M45r	968.6		169.7	

result is a lesser number of blocks in the composite polarity model. In contrast, the numerous profiles in the H801 survey allowed many short-wavelength anomalies to be correlated in that area.

4. Discussion

[34] In this study, we correlated and modeled deep-tow magnetic anomaly profiles in the Pacific JQZ using new data to complement previous deep-tow profiles collected in this area [*Sager et al.*, 1998]. These new data augment the previous study in several ways. Closely spaced lines allow for a detailed correlation of short-wavelength anomalies in two areas: one around M34 and the other at ODP Hole 801C. The new data also provide additional information in areas of uncertain anomaly correlations (NORTH) as well as extending the JQZ deep-tow survey across Hole 801C to the RSB [*Handschumacher et al.*, 1988] (SOUTH). Additional data allow us to address several questions about the JQZ: (1) Are the shortest-wavelength anomalies mapped in previous JQZ studies correlatable? (2) Are correlatable anomalies found further back in time within the JQZ? (3) Are apparent reversals in the 474-m basalt section cored at Hole 801C representative of surrounding magnetic lineations? (4) What are the implications for the cause of JQZ?

4.1. Anomaly Correlation

[35] Closely spaced deep-tow magnetic profiles in the M34 and H801 surveys show good to excellent correlation (i.e., similarity in terms of shape, position, and size) of both short- and long-wavelength anomalies. Although not quite as robust, partly owing to having only two profiles, correlation of anomalies in the SOUTH survey is also good as is the correlation of anomalies in the northern part of the Pigafetta JQZ, from M36 northwestward to M27 [*Handschumacher et al.*, 1988; *Sager et al.*, 1998]. For these age sequences, the correlation of anomalies on adjacent lines strongly suggests that the anomalies are linear, especially given the linearity of the anomalies in the two small surveys with closely spaced lines (M34 and H801). Thus, on the whole, the JQZ anomalies appear similar to other linear magnetic anomalies around the world that are attributed to magnetic reversals recorded by the process of seafloor spreading and crustal construction at midocean ridges.

[36] In contrast, anomaly correlations are poor in the ~300-km long LAZ. This section has the smallest amplitude anomalies measured and as previously noted is a zone

Table 2. Midwater Geomagnetic Polarity Reversal Timescale Model

	Distance (km)		Age (Ma)	
Chron	Young	Old	Young	Old
M37r	451.5	472.8	162.0	162.3
M38n1r	480.4	485.2	162.5	162.6
M38n2r	492.3	498.3	162.6	162.7
M38n3r	504.1	512.1	162.8	162.9
M38n4r	528.3	537.3	163.2	163.3
M38r	543.5	555.9	163.4	163.6
M39n1r	562.5	583.5	163.7	164.0
M39n2r	614.9	625.7	164.5	164.6
M39n3r	630.6	641.9	164.7	164.9
M39n4r	647.6	655.0	164.9	165.1
M39n5r	659.4	665.7	165.1	165.2
M39r	671.6	677.5	165.3	165.4
M40n1r	680.9	689.6	165.4	165.6
M40n2r	697.6	703.8	165.7	165.8
M40r	706.9	732.2	165.8	166.2
M41n1r	736.3	739.6	166.3	166.3
M41n2r	742.1	744.7	166.4	166.4
M41r	755.3	781.3	166.6	166.9
M42n1r	790.6	811.3	167.1	167.4
M42n2r	817.7	823.1	167.5	167.6
M42n3r	831.9	833.9	167.7	167.7
M42r	850.7	860.6	167.9	168.1
M43n1r	864.5	880.7	168.2	168.4
M43n2r	888.8	897.5	168.5	168.7
M43r	905.3	914.9	168.8	168.9
M44n1r	931.7	961.2	169.2	169.6
M44n2r	971.3		169.8	

of difficult correlation [*Handschumacher et al.*, 1988; *Sager et al.*, 1998]. Although the closely spaced tracks around Hole 801C illustrate that small anomalies can be successfully correlated, similar anomalies in the LAZ are difficult to match with the same certainty. One characteristic that makes anomalies in this zone difficult to correlate is the mismatch of large, long wavelength anomalies. Although the two older deep-tow profiles have similar long-wavelength anomalies (indeed, *Sager et al.* [1998] used these anomalies as a guide for correlating the smaller anomalies) the new deep-tow profile in between has a different long wavelength appearance. The source of the long-wavelength anomalies is uncertain. Given the observed mismatch, they do not appear linear in the LAZ. A possible cause is magnetic overprinting by the Mid-Cretaceous volcanism that usually appears as sills intruded into the sediments. In this area, this volcanism appears patchy [*Abrams et al.*, 1993] as do the larger magnetic anomalies. Furthermore, the small-amplitude, short-wavelength character of the LAZ anomalies implies that they may have other causes. For example, the magnetic field may have had rapid reversals or fluctuations that were too frequent to make strongly linear anomalies or the magnetic recording was degraded because of ridge jumps, propagating rifts or later volcanic activity. Currently, we do not have sufficient data to determine whether these anomaly characteristics in the LAZ result from geomagnetic field or volcanic artifacts.

4.2. Polarity Reversal Models

[37] We constructed a magnetization model of the deep-tow anomaly profiles to help understand the nature of the anomalies. The assumption of alternating blocks of opposite polarity is convenient for modeling, although we do not know which of these small anomalies results from a magnetic field reversal and which is simply a field intensity or directional fluctuation. Thus, taking the next step of assigning ages and representing the sequence as a GPTS, has inherent risks. Correlations of some anomalies is poor and even those with apparently good correlations in our geographically restricted data set do not demonstrate that the observed pattern has global repeatability and significance. Nevertheless, we present a GPTS model here for two reasons. It is a natural extension of previous work that allows the reader to better understand the implications of this study relative to those preceding it. More importantly, progress in developing a Jurassic GPTS requires it. The current mid-Jurassic to Early Cretaceous GPTS is based on *Handshumacher et al.* [1988] and *Sager et al.* [1998]. Although the GPTS from this study contains uncertainties because of the small number of profiles, the limited extent, and the LAZ correlation difficulties, it is a template for magnetostratigraphic work and studies of JQZ anomalies elsewhere. Thus, in this study, we are obliged to consider the implications of the GPTS.

[38] In building reversal models of the deep tow magnetic lines, we made the traditional assumption that all significant anomalies result from magnetic reversals recorded by the seafloor spreading process [*Vine and Matthews*, 1963]. Although this assumption has been highly successful in creating GPTS models, several studies suggest that small anomalies may not always represent polarity reversals [e.g., *Cande and Kent*, 1992b; *Bowles et al.*, 2003]. An alternative to interpreting all anomalies as reversals is to consider that some of them could be due to fluctuations of paleofield intensity and magnetic field excursions (i.e., incomplete reversals). Statistically, reversals, excursions, and paleointensity fluctuations probably result from the same set of geomagnetic instabilities, implying that they would appear similar in magnetic profile data [*Marzocchi*, 1997]. The nonuniqueness of potential field modeling does not allow us to determine which small anomalies represent true polarity reversals and which are simply magnetic field fluctuations. For their widely accepted GPTS model, *Cande and Kent* [1992a, 1992b] rejected polarity chrons with durations shorter than 30 ka as likely to result from paleointensity fluctuations. Similarly, *Sager et al.* [1998] constructed a Jurassic GPTS with a reversal for every magnetic anomaly but preferred a model filtered by upward continuation to midwater depth because it retained reversals only for the longer-wavelength anomalies.

[39] To distinguish between reversals and field fluctuations, several investigator groups have compared sedimentary magnetostratigraphy with "cryptochrons" (i.e., small anomalies of uncertain cause in magnetic profiles). *Lanci and Lowrie* [1997] suggested that cryptochrons within C12 and C13 in the timescale of *Cande and Kent* [1995] are paleointensity fluctuations rather than magnetic reversals because of a lack of corresponding polarity reversals in contemporaneous sediment cores. Similar conclusions were reached for small anomalies within chron C5 on the basis of a strong correlation between deep-tow magnetic profiles and sedimentary relative paleointensity records [*Bowers et al.*, 2001; *Bowles et al.*, 2003]. In contrast, *Roberts and Lewin-Harris* [2000] concluded that small anomalies in chron C5 result from polarity reversals, suggesting that even when

high-resolution sedimentary data are available, the interpretation of such data may not be straightforward. Furthermore, some investigators have concluded that the resolution of sedimentary paleomagnetic records depends significantly on sedimentation rate and small anomalies can be averaged out if the sedimentation rate is not high enough [*Roberts and Winklhofer*, 2004]. Thus, the fidelity of sedimentary records may be verified only when the records show consistency at several sites around the world.

[40] With our data set, consisting of magnetic profiles only, it is not possible to make a definitive interpretation of the source of small magnetic anomalies observed in the Pacific JQZ. Consequently, we simply constructed a Jurassic GPTS assuming that those anomalies larger than ~1.2 km wavelength (the smaller being noise) observed with the deep-tow magnetometer are caused by blocks of contrasting polarity.

[41] As did *Sager et al.* [1998] for their model of the JQZ polarity reversal sequence, we prefer the model made from magnetic anomalies upward continued to midwater level because the upward continuation filters out many of the shortest-wavelength features and gives results comparable to sea surface magnetic data near the present-day mid-ocean ridges. The deep-tow magnetic profiles show many short-wavelength features, some of which may result from phenomena other than magnetic reversals.

[42] Several factors indicate that the GPTS must be treated with caution. Correlations are uncertain in some portions, especially the LAZ. It is impossible to determine, from magnetic profiles alone, whether small anomalies are caused by reversals. Furthermore, models made at different levels show differences related to the changing appearance of the anomalies when upward continued.

4.3. Correlation of Models and Hole 801C Log Data

[43] Despite ambiguities about the interpretations of reversals in our GPTS models, two independent types of data, magnetic data from Hole 801C and Jurassic magnetic stratigraphy studies from continental sedimentary sections, support the existence of many short polarity periods, implying a rapid reversal frequency. Paleomagnetic and downhole logging data are available from the 474-m basalt section cored at Hole 801C. Both data sets imply six reversals in the section [*Wallick and Steiner*, 1982; *Steiner*, 2001; *Tivey et al.*, 2005]. Four polarity changes are found within the upper, 150-m, off axis lava sequence while two polarity changes are found within the lower lava sequence, which was presumably accreted at or near the spreading axis. Formation microscanner (FMS) log data show significant dips in the lava sequences within the hole [*Pockalny and Larson*, 2003]. If the tilted lava sequence boundaries indicate that magnetization boundaries are similarly tilted, then changes in magnetic polarity can occur within a vertical hole [*Tivey et al.*, 2005]. The multiple polarities of the upper off-axis lava sequence also implies rapid polarity reversal rate ~7 Ma after the main crustal accretion occurred (167.4 Ma), which is consistent with the rapidly reversing field at M34 age (160 Ma). These observations along with the lineated character of magnetic anomalies around Hole 801C suggest that seafloor spreading has recorded rapid polarity reversals during this time period and the small anomalies are not just the signal of geomagnetic field intensity fluctuations.

[44] The finding of multiple polarity sections within the Hole 801C section is suggestive of a high reversal rate; however, the actual rate is difficult to estimate because of uncertainties about crustal architecture and accretion rates. Within M42 on our GPTS model (Figure 11), corresponding to the H801 survey area, the −5.5 km model implies a reversal rate of ~26 rev/Ma (1 rev/38 ka). Alternatively, the −3.0 km model (Figure 11), which leaves out the smallest anomalies, gives only ~8 rev/Ma (1 rev/125 ka).

[45] The highest reversal rates for the accepted GPTS occurred during the Miocene, ~10 Ma, with a rate of ~5 rev/Ma. This is not greatly different from the lowest rates implied by the deep-tow magnetic profile models and implies that the lower of inferred JQZ rates are not extreme. Furthermore, similar rates (~6–8 rev/Ma) have been also interpreted from Jurassic continental magnetostratigraphic studies [*Steiner et al.*, 1987; *Steiner*, 2001; J. Ogg, personal communication, 2004]. Our deep-tow GPTS model is therefore consistent with largely independent observations that imply many short polarity reversals during the Jurassic.

4.4. Cause of the JQZ

[46] Pacific JQZ deep-tow magnetic data provide a high-resolution recording of apparently unusual geomagnetic field behavior during the Jurassic. Although magnetic anomalies are nonunique and by themselves do not provide an unequivocal explanation for the JQZ, the data from this study give important clues about the factors involved. Generally, our inferences follow from systematic variations in the JQZ anomaly sequence and comparisons with independent data.

[47] Systematic changes in anomaly amplitudes are observed along the deep-tow lines. Anomaly amplitude decreases with increasing age (i.e., toward the southeast) continuing the trend that has been noted by other authors [e.g., *Cande et al.*, 1978; *Sager et al.*, 1998; *McElhinny and Larson*, 2003; *Tivey et al.*, 2006], reaching a minimum amplitude and shortest wavelength in the LAZ (Figure 10), tentatively identified as being between M38 and M41. At older ages (i.e., farther southeast), anomaly amplitudes increase slightly south of Hole 801C. This trend is also seen in the modeled magnetization values (section 2.3), which decrease from M34 (3.9 Am^{-1}) to NORTH (2.0 Am^{-1}) and increase from H801C (1.7 Am^{-1}) to SOUTH (2.3 Am^{-1}). Although we used a constant thickness for the magnetic source layer for modeling, an alternative is to consider these systematic changes as a result of changes in source layer thickness, rather than variations in the geomagnetic field. We think this explanation is unlikely because of the large implied changes in source layer thickness. For example, to reproduce the anomaly amplitudes observed in the M34 and H801C areas with same magnetization value (e.g., 2.0 Am^{-1}), the source layer thickness of M34 and H801C must be different by a factor >3 (0.7 and 3.0 km, for M34 and H801C, respectively). This much variation within fast spreading mid-ocean ridge crust with a flat seafloor topography is unlikely. Instead, following similar interpretations of the global magnetic anomaly sequence [e.g., *McElhinny and Larson*, 2003], changes in JQZ anomaly amplitude imply changes in paleomagnetic

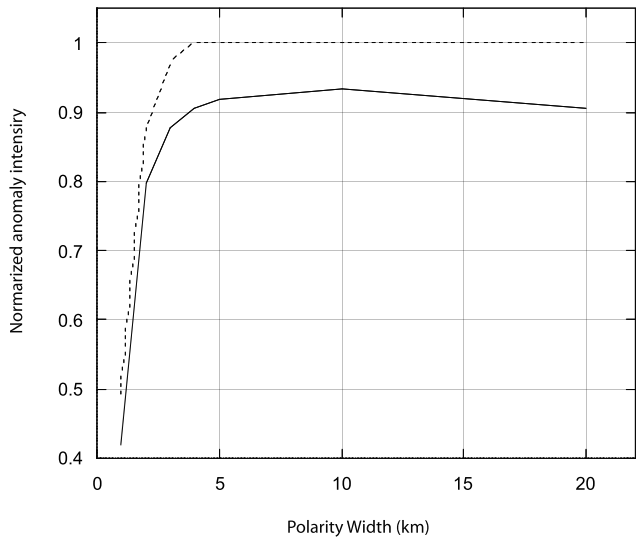

Figure 12. Curves showing decline in model anomaly amplitudes for small-width polarity blocks owing to lateral interference. Vertical axis is normalized model magnetic anomaly amplitude. Horizontal axis is width of polarity block. Dotted line is model with vertical polarity block boundaries; solid line is model with dipping (53°) lateral boundaries.

field strength, perhaps related to reversal rate. The field intensity seems to have decreased until reaching a minimum during the LAZ, where the fluctuation rate appears highest, and then increased through the late Jurassic as reversal rate declined [*Tivey et al.*, 2006].

[48] Changes in anomaly amplitude on the deep-tow profiles, particularly around the LAZ, may give clues about the origin of the JQZ. We consider several hypotheses that may partly or completely explain the observed changes: (1) long-term decrease in crustal magnetization as a result of either alteration or decreased dipole field intensity, (2) low transitional field intensities combined with rapid reversals, (3) interference of the magnetic anomalies caused by closely spaced polarity blocks in the oceanic crust, and (4) a tectonic disruption in the LAZ perhaps caused by spreading ridge reorientation and/or propagation.

[49] A decrease of crustal magnetizationgoing backward in time has been documented for the past 30 Ma and attributed to progressive alteration [*Johnson and Pariso*, 1993]. This explanation does not seem likely for the JQZ because existing evidence implies that changes in magnetization beyond ~30 Ma due to alteration are small [*Johnson and Pariso*, 1993]. More likely is that the overall decrease in anomaly amplitude [e.g., *McElhinny and Larson*, 2003] is a global phenomenon related to a decrease of geomagnetic field strength. Independent, paleomagnetic data imply that the Jurassic was a time of low dipole field strength (so-called "Mesozoic dipole low") [e.g., *Prévot et al.*, 1990; *McElhinny and McFadden*, 2000; *Thomas and Biggin*, 2003; *Biggin and Thomas*, 2003].

[50] One possible explanation for the LAZ is that the geomagnetic field was weaker than normal during the LAZ because of rapid reversals and overlapping transitional field minima. It is well-known that the dipole field is reduced during geomagnetic field reversals, perhaps only to ~25% of the nonreversing dipole field strength [*Merrill and McFadden*, 1999]. Furthermore, it is thought that periods of weaker field intensity are characterized by greater numbers of reversals and excursions [*Valét et al.*, 2005]. Thus, we might expect that a period containing many, closely spaced reversals may also be a time of reduced field strength, perhaps because periods of transition field minima overlap (i.e., the field does not regain full strength before starting another reversal). At face value, our deep-tow GPTS for the LAZ implies only a reversal rate of ~10 rev/Ma. This is not much higher than inferred Miocene reversal rates and implies an average time between reversals of ~100 ka. If transitional field minima have durations of less than ~10 ka [*Merrill and McFadden*, 1999], the overlap from polarity periods of the implied duration would be minimal. However, if field minima are broader (e.g., 60–80 ka) [*Valét et al.*, 2005] or the reversal rate is substantially higher, overlapping field minima may be part of the reason for the apparent low LAZ anomaly amplitudes. Reversal rates in the LAZ may be significantly higher than implied by our GPTS because this model contains only the better-correlated ano-malies in a zone of poor correlation. If all anomalies are interpreted as a result of polarity reversals, the model for deep-tow lines 3-9, 4-1 implies a reversal rate of ~12 rev/Ma (Figure 10), with an average period of ~82 ka between transitions.

[51] Another potential factor causing the LAZ is overlapping and partially canceling magnetic anomalies caused by closely spaced blocks of opposing polarity. To judge the plausibility of this hypothesis, we calculated simple 2-D forward models [*Talwani and Heirtzler*, 1964] of crustal anomalies and tested the reduction of anomaly amplitude with different spacing of opposing polarity blocks. For simplicity, we assumed a 1 km thickness for the source layer, a distance of 500 m between the top of the source and the observation plane (similar to the TN152 deep-tow magnetometer geometry), and sharp boundaries between polarity blocks (i.e., transition width of zero). Models were made at different reversal rates, which varied the width of the polarity blocks. We also made two different models of the polarity boundaries, one with vertical boundaries and another with boundaries tilting 53° from vertical (the tilt angle inferred for Hole 801C layers by *Pockalny and Larson* [2003]). Overall, the intensity of anomalies from the tilted-boundary model is less than those of the nontilted model (Figure 12), presumably because the tilted blocks produce greater overlap of opposing polarity material. A similar result would be given with finite-width polarity transitions. Most importantly, the models show a precipitous drop in anomaly amplitudes when the polarity boundaries are less than ~4 km apart and this result is approximately the same for both tilted and non-tilted polarity block boundaries. This finding implies that even at deep-tow depths, there can be a significant reduction in anomaly amplitude caused by small-width polarity blocks. In some portions of the LAZ, small anomalies imply polarity blocks 4 km or less in width. Thus, the partial cancellation of overlapping anomalies may be a factor reducing LAZ anomaly amplitudes.

[52] The poor correlation of LAZ anomalies may also result wholly or in part from tectonic and/or crustal accre-

tion complications. If there were tectonic complexities, such as ridge jumps, propagating ridges, or microplate rotations, we could expect disturbed, difficult-to-correlate anomalies to be the result. One complication could be the superposition of lavas of differing ages owing to off-axis eruptions. Cores from Hole 801C show both an off-axis lava eruption and a late-stage akalic eruptions [*Koppers et al.*, 2003a, 2003b; *Tivey et al.*, 2005]. Neither of these later eruptions appears to have significantly degraded the correlation of magnetic anomalies around Hole 801, even though they represent a hiatus in crustal accretion that is much longer than the apparent reversal period. This suggests that the Hole 801C primary magnetic layer is not significantly affected by the later eruptions. However, at another site, such as the LAZ, later igneous activity may have confounded the crustal anomaly signal. Another possible complication is tectonic reorganization, such as ridge realignment, ridge jumps, propagating rifts, or microplate formation. Owing to the paucity of well-defined magnetic lineations regionally, the history of Jurassic seafloor spreading in the Pacific is poorly known. Because the JQZ magnetic anomalies are only well-defined in the deep-tow data, we cannot be certain of the tectonic setting and history of surrounding areas and thus the contribution of tectonics to the observed magnetic record is unclear and difficult to evaluate. Ultimately, to be accepted as representative of global magnetic field phenomena, the results from the LAZ in particular, and Pacific JQZ in general, must be corroborated with independent data from the two other lineation sets in the Pacific and other regions in the world oceans.

5. Conclusions

[53] In this study, we present ~1550 km of new deep-tow magnetic profiles from the Pacific JQZ and two revised Jurassic GPTS models that complement and extend a previous study [*Sager et al.*, 1998]. Many of the surveyed anomalies appear to correlate well and are considered to be true magnetic lineations recorded by the seafloor spreading process. This conclusion is bolstered by deep-tow magnetic anomalies resolved in two small survey areas with multiple overlapping lines that show excellent correlation and linearity and a similarity to Hole 801C downhole results. In contrast, the origin of difficult-to-correlate, high-frequency anomalies in the middle of the study area (i.e., LAZ area) is less certain.

[54] We constructed a polarity block model in which all of the correlated deep-tow magnetic anomalies are assumed to result from geomagnetic polarity reversals and the result is a JQZ GPTS model extending from anomaly M30 to M45 (~157.8 to 169.7 Ma). We also derived a GPTS model for profiles upward continued to midwater levels. This GPTS shows fewer polarity periods but is more comparable to Cenozoic and late Cretaceous GPTS derived from magnetic data with a similar source-sensor separation. The deep-tow GPTS is likely an overestimation of the true number of polarity reversals because it probably includes anomalies caused by geomagnetic field fluctuations that were incorrectly interpreted as reversals. Furthermore, the LAZ portion of the GPTS model (M37-M41) is uncertain because of poor correlation in that region. Nevertheless, the GPTS provides a template for future JQZ polarity reversal studies.

[55] Although the average implied reversal rate for the deep-tow GPTS is ~12 rev/Ma, the model around Hole 801C implies rates twice that high, if all anomalies are interpreted as reversals. Such values are similar to rates implied by studies from drilling data from Hole 801C, bolstering the argument that many of the deep-tow magnetic anomalies in the vicinity of Hole 801C result from geomagnetic polarity reversals. This conclusion is also consistent with findings of rapid polarity reversals from continental magnetostratigraphy studies for the Jurassic.

[56] Changes in deep-tow profile anomaly amplitudes give clues about the origin of the JQZ. Anomaly amplitudes decrease with age into the LAZ and then increase slightly, suggesting that the LAZ was a period of abnormal, low field intensity. The decrease of anomaly amplitudes is consistent with independent results indicating that the Jurassic was a time of weak geomagnetic field strength (the Mesozoic dipole low) and implies a global geomagnetic field contribution to low anomaly amplitudes within the JQZ. We examined several additional hypotheses to explain the LAZ and favor a combination of reduced field intensity, perhaps caused or augmented by overlapping transitional field minima, along with interference and partial anomaly cancellation owing to closely spaced, narrow polarity blocks. Tectonic complications are also a possible contributor for the poor correlation of LAZ anomalies, but this contribution cannot be evaluated without better knowledge of local Pacific Jurassic tectonics.

[57] **Acknowledgments.** We thank the captain and crew of the R/V *Thomas G. Thompson* and technicians of the Woods Hole Deep-Submergence Operations Group and the Hawaii Mapping Research Group for making it possible to carry out a successful TN152 cruise. We are greatly in debt to Roger Larson, who passed away as this manuscript was being prepared. Roger's work in Pacific tectonics and the GPTS inspired and shaped this research. He was a reviewer for the proposal for this study as well as manuscripts from this and other similar research. Indeed, we always wrote with Roger in mind, knowing that we would have to answer to his insightful mind and broad range of knowledge. This research was supported by the National Science Foundation grants OCE-0099161 and OCE-0099237. Tominaga was partly supported by funds from the Jane and R. Ken Williams '45 Chair in Ocean Drilling Science, Education, and Technology.

References

Abrams, L. J., R. L. Larson, T. H. Shipley, and Y. Lancelot (1993), Cretaceous volcanic sequences and Jurassic oceanic crust in the east Mariana and Pigafetta basins of the western Pacific, in *The Mesozoic Pacific: Geology, Tectonics, and Volcanism*, Geophys. Monogr. Ser, vol. 77, edited by M. S. Pringle et al., pp. 77–101, AGU, Washington, D. C.

Barrett, D. L., and C. E. Keen (1976), Mesozoic magnetic lineations, the magnetic quiet zone, and sea floor spreading in the northwest Atlantic, *J. Geophys. Res.*, *81*, 4875–4884, doi:10.1029/JB081i026p04875.

Biggin, A. J., and D. N. Thomas (2003), Analysis of long-term variations in the geomagnetic poloidal field intensity and evaluation of their relationship with global geodynamics, *Geophys. J. Int.*, *152*, 392–415, doi:10.1046/j.1365-246X.2003.01849.x.

Bowers, N. E., S. C. Cande, J. S. Gee, A. Hildebrand, and R. L. Parker (2001), Fluctuations of the paleomagnetic field during Chron C5 as recorded in near-bottom marine magnetic anomaly data, *J. Geophys. Res.*, *106*, 26,379–26,396, doi:10.1029/2001JB000278.

Bowles, J., L. Tauxe, J. Gee, D. McMillan, and S. Cande (2003), Source of tiny wiggles in Chron C5: A comparison of sedimentary relative intensity and marine magnetic anomalies, *Geochem. Geophys. Geosyst.*, *4*(6), 1049, doi:10.1029/2002GC000489.

Cande, S. C., and D. V. Kent (1992a), A new geomagnetic polarity time scale for the Late Cretaceous and Cenozoic, *J. Geophys. Res.*, *97*, 13,917–13,951, doi:10.1029/92JB01202.

Cande, S. C., and D. V. Kent (1992b), Ultrahigh resolution marine magnetic anomaly profiles: A record of continuous paleointensity variations?, *J. Geophys. Res.*, *97*, 15,075–15,083, doi:10.1029/92JB01090.

Cande, S. C., and D. V. Kent (1995), Revised calibration of the geomagnetic polarity timescale for the late Cretaceous and Cenozoic, *J. Geophys. Res.*, *100*, 6093–6095, doi:10.1029/94JB03098.

Cande, S. C., J. L. LaBrecque, and R. L. Larson (1978), Magnetic anomalies in the Pacific Jurassic Quiet Zone, *Earth Planet. Sci. Lett.*, *41*, 434–440, doi:10.1016/0012-821X(78)90174-7.

Channell, J. E. T., E. Erba, M. Nakanishi, and K. Tamaki (1995), Late Jurassic-Early Cretaceous time scales and oceanic magnetic anomaly block models, in *Geochronology, Time Scales, and Global Stratigraphic Correlation: A Unified Temporal Framework for a Historical Geology*, edited by W. A. Berggren et al., *SEPM Spec. Publ.*, *54*, 51–63.

Gradstein, F. M., F. Agterberg, J. G. Ogg, J. Hardenbol, P. van Veen, J. Thierry, and Z. Huang (1995), A Triassic, Jurassic, Jurassic and Cretaceous time scale, in *Geochronology, Time Scales and Global Stratigraphic Correlations: A Unified Temporal Framework for a Historical Geology*, edited by W. A. Berggren et al., *SEPM Spec. Publ.*, *54*, 95–126.

Guspi, F. (1987), Frequency-domain reduction of potential field measurements to a horizontal plane, *Geoexploration*, *24*, 87–89, doi:10.1016/0016-7142(87)90083-4.

Handschumacher, D. W., W. W. Sager, T. W. C. Hilde, and D. R. Bracey (1988), Pre-Cretaceous tectonic evolution of the Pacific plate and extension of the geomagnetic polarity reversal timescale with implications for the origin of the Jurassic "Quiet Zone", *Tectonophysics*, *155*, 365–380, doi:10.1016/0040-1951(88)90275-2.

Hayes, D. E., and P. D. Rabinowitz (1975), Mesozoic magnetic lineations and the magnetic quiet zone off northwest Africa, *Earth Planet. Sci. Lett.*, *28*, 105–115, doi:10.1016/0012-821X(75)90217-4.

Heirtzler, J. R., and D. E. Hayes (1967), Magnetic boundaries in the north Atlantic Ocean, *Science*, *157*, 185–187, doi:10.1126/science.157.3785.185.

Johnson, H. P., and J. E. Pariso (1993), Variations in oceanic crustal magnetization: Systematic changes in the last 160 million years, *J. Geophys. Res.*, *98*, 435–445, doi:10.1029/92JB01322.

Koppers, A. A. P., H. Staudigel, and R. A. Duncan (2003a), High-resolution Ar/Ar dating for the oldest oceanic basement basalts in the western Pacific basin, *Geochem. Geophys. Geosyst.*, *4*(11), 8914, doi:10.1029/2003GC000574.

Koppers, A. A. P., H. Staudigel, M. S. Pringle, and J. R. Wijbrans (2003b), Short-lived and discontinuous intraplate volcanism in the South Pacific: Hot spots or extensional volcanism?, *Geochem. Geophys. Geosyst.*, *4*(10), 1089, doi:10.1029/2003GC000533.

Lancelot, T., and R. L. Larson (1990), Site 801, *Proc. ODP Init. Rep.*, *129*, 91–170.

Lanci, L., and W. Lowrie (1997), Magnetostratigraphic evidence that 'tiny wiggles' in the oceanic magnetic anomaly record represent geomagnetic paleointensity variations, *Earth Planet. Sci. Lett.*, *148*, 581–592, doi:10.1016/S0012-821X(97)00055-1.

Larson, R. L., and T. W. C. Hilde (1975), A revised time scale of magnetic reversals for the Early Cretaceous and late Jurassic, *J. Geophys. Res.*, *80*, 2586–2594, doi:10.1029/JB080i017p02586.

Larson, R. L., and W. C. Pitman III (1972), World-wide correlation of Mesozoic magnetic anomalies and its implications, *Geol. Soc. Am. Bull.*, *83*, 3645–3662, doi:10.1130/0016-7606(1972)83[3645:WCOMMA]2.0.CO;2.

Larson, R. L., and W. W. Sager (1992), Skewness of magnetic anomalies M0 to M29 in the northwestern Pacific, *Proc. ODP Sci. Res.*, *129*, 471–481.

Larson, R. L., and S. O. Schlanger (1981), Geological evolution of the Nauru basin, and regional implications, *Init. Rep. DSDP*, *61*, 533–548.

Larson, R. L., M. B. Steiner, E. Erba, and Y. Lancelot (1992), Paleolatitudes and tectonic reconstructions of the oldest portion of the Pacific plate: A comparative study, *Proc. ODP Sci. Res.*, *129*, 615–631.

Ludden, J. (1992), Radiometric age determinations for basement from Site 765 and 766, Argo abyssal plain and north western Australia, *Proc. ODP Sci. Res.*, *123*, 557–559.

Marzocchi, W. (1997), Missing reversals in the geomagnetic polarity timescale: Their influence on the analysis and in constraining the process that generates geomagnetic reversals, *J. Geophys. Res.*, *102*, 5157–5171, doi:10.1029/96JB03594.

McElhinny, M. W., and R. L. Larson (2003), Jurassic dipole low defined from land and sea data, *Eos Trans. AGU*, *84*, 362–366.

McElhinny, M. W., and P. L. McFadden (2000), *Paleomagnetism: Continents and Oceans*, 368 pp., Academic, San Diego, Calif.

Merrill, R. T., and P. L. McFadden (1999), Geomagnetic polarity transitions, *Rev. Geophys.*, *37*, 201–226, doi:10.1029/1998RG900004.

Nakanishi, M., K. Tamaki, and K. Kobayashi (1989), Mesozoic magnetic anomaly lineations and seafloor spreading history of the northwestern Pacific, *J. Geophys. Res.*, *94*, 15,437–15,462, doi:10.1029/JB094iB11p15437.

Nakanishi, M., K. Tamaki, and K. Kobayashi (1992), Mesozoic magnetic lineations from late Jurassic to Early Cretaceous in the west central Pacific Ocean, *Geophys. J. Int.*, *109*, 701–719, doi:10.1111/j.1365-246X.1992.tb00126.x.

Nwogbo, P. O. (1998), Spectral prediction of magnetic source depths from simple numerical models, *Comput. Geosci.*, *24*, 847–852, doi:10.1016/S0098-3004(97)00131-3.

Ogg, J. G., and J. Gutowski (1995), Oxfordian magnetic polarity time scale, in *Proceedings of the 4th International Congress on Jurassic Stratigraphy and Geology, Geo. Res. Forum,* vol. 1–2, edited by A. C. Riccardi, pp. 406–414, Trans-Tec Publ., Zurich, Switzerland.

Ogg, J. G., M. B. Steiner, F. Oloriz, and J. M. Tevera (1984), Jurassic magnetostratigraphy, 1. Kimmeridgian-Tithonian of Sierra Gorda and Carcabuey, southern Spain, *Earth Planet. Sci. Lett.*, *71*, 147–162, doi:10.1016/0012-821X(84)90061-X.

Ogg, J. G., M. B. Steiner, J. Wieczorek, and M. Hoffman (1991), Jurassic magnetostratigraphy, 4. Early Callovian through Middle Oxfordian of the Krakow Uplands (Poland), *Earth Planet. Sci. Lett.*, *104*, 488–504, doi:10.1016/0012-821X(91)90224-6.

Olsen, N., T. J. Sabaka, and L. Toffner-Clausen (2000), Determination of the IGRF 2000 model, *Earth Planets Space*, *52*, 1175–1182.

Onwumechili, C. A. (1967), Geomagnetic variations in the equatorial zone, in *Physics of Geomagnetic Phenomena*, edited by S. Matsushita and W. H. Campbell, pp. 452–507, Academic, San Diego, Calif.

Parker, R. L. (1972), The rapid calculation of potential field anomalies, *Geophys. J.R. Astron. Soc.*, *31*, 447–455.

Parker, R. L. (1997), Coherence of signals from magnetometers on parallel paths, *J. Geophys. Res.*, *102*, 5111–5117, doi:10.1029/96JB03803.

Parker, R. L., and S. P. Huestis (1974), The inversion of magnetic anomalies in the presence of topography, *J. Geophys. Res.*, *79*, 1587–1593, doi:10.1029/JB079i011p01587.

Plank, T., J. N. Ludden, and C. Escutia, and the Shipboard Scientific Party (2000), Site 801, *Proc. ODP Init. Repts., 185* [CD-ROM], Ocean Drilling Program, Texas A&M Univ., College Station, Tex.

Pockalny, R. A., and R. L. Larson (2003), Implications for crustal accretion at fast spreading ridges from observations in Jurassic oceanic crust in the western Pacific, *Geochem. Geophys. Geosyst.*, *4*(1), 8903, doi:10.1029/2001GC000274.

Prévot, M., M. E. Derder, M. McWilliams, and J. Thompson (1990), Intensity of the Earth's magnetic field: Evidence for a Mesozoic dipole low, *Earth Planet. Sci. Lett.*, *97*, 129–139, doi:10.1016/0012-821X(90)90104-6.

Roberts, A. P., and J. C. Lewin-Harris (2000), Marine magnetic anomalies: Evidence that 'tiny wiggles' represent short-period geomagnetic polarity intervals, *Earth Planet. Sci. Lett.*, *183*, 375–388, doi:10.1016/S0012-821X(00)00290-9.

Roberts, A. P., and M. Winklhofer (2004), Why are geomagnetic excursions not always recorded in sediments? Constraints from post-depositional remanent magnetization lock-in modeling, *Earth Planet. Sci. Lett.*, *227*, 345–359, doi:10.1016/j.epsl.2004.07.040.

Roeser, H. A., C. Steiner, B. Schreckenberger, and M. Block (2002), Structual development of the Jurassic Magnetic Quiet Zone off Morocco and identification of Middle Jurassic magnetic lineations, *J. Geophys. Res.*, *107*(B10), 2207, doi:10.1029/2000JB000094.

Sager, W. W., C. J. Weiss, M. A. Tivey, and H. P. Johnson (1998), Geomagnetic polarity reversal model of deep-tow profiles from the Pacific Jurassic Quiet Zone, *J. Geophys. Res.*, *103*, 5269–5286, doi:10.1029/97JB03404.

Schlanger, S. O., H. C. Jenkyns, and I. Premoli-Silva (1981), Volcanism and vertical tectonics in the Pacific basin related to global transgressions, *Earth Planet. Sci. Lett.*, *52*, 435–449, doi:10.1016/0012-821X(81)90196-5.

Schouten, H., and C. R. Denham (1979), Modeling the oceanic magnetic source layer, in *DSDP Results in the Atlantic Ocean: Ocean Crust*, Maurice Ewing Symp, vol. 2, edited by M. Talwani, C. G. A. Harrison, and D. E. Hayes, pp. 151–159, AGU, Washington, D. C.

Spector, A., and F. S. Grant (1970), Statistical models for interpreting aeromagnetic data, *Geophysics*, *35*, 293–302, doi:10.1190/1.1440092.

Steiner, M. B. (1980), Investigation of the geomagnetic field polarity during the Jurassic, *J. Geophys. Res.*, *85*, 3572–3586, doi:10.1029/JB085iB07p03572.

Steiner, M. B. (2001), Tango in the Mid-Jurassic: 10,000-Yr geomagnetic field reversals, *Eos Trans. AGU*, *82*(47), Fall Meet. Suppl., Abstract GP12A-0205.

Steiner, M. B., J. G. Ogg, G. Melendez, and L. Sequeiros (1985), Jurassic magnetostratigraphy, 2. Middle-Late Oxfordian of Aguilon, Iberian Cordillera, northern Spain, *Earth Planet. Sci. Lett.*, *76*, 151–166, doi:10.1016/0012-821X(85)90155-4.

Steiner, M. B., J. Ogg, and J. Sandoval (1987), Jurassic magnetostratigraphy, 3. Bathonian-Bjocian of Carcabuey, Sierra Harana and Campillo de Arenas

(Subbetic Cordillera, soutern), *Earth Planet. Sci. Lett.*, *82*, 357–372, doi:10.1016/0012-821X(87)90209-3.

Talwani, M., and J. R. Heirtzler (1964), Computation of magnetic anomalies caused by two-dimensional structures of arbitrary shape, in *Computers in the Mineral Industries*, edited by G. A. Parks, pp. 464–480, Stanford Univ. Press, Stanford, Calif.

Thomas, D. N., and A. J. Biggin (2003), Does the Mesozoic dipole low really exist?, *Eos Trans. AGU*, *84*(97), 103–104.

Tivey, M. A., R. L. Larson, H. Schouten, and R. Pockalny (2005), Downhole magnetic measurements of ODP Hole 801C: Implications for Pacific oceanic crust and magnetic field behavior in the Middle Jurassic, *Geochem. Geophys. Geosyst.*, *6*, Q04008, doi:10.1029/2004GC000754.

Tivey, M. A., W. W. Sager, S. Lee, and M. Tominaga (2006), The origin of the Pacific Jurassic Quiet Zone, *Geology*, *34*(9), 789–792, doi:10.1130/G22894.1.

Valét, J.-P., L. Meynadier, and Y. Guyodo (2005), Geomagnetic dipole strength and reversal rate of the past two million years, *Nature*, *435*, 802–804, doi:10.1038/nature03674.

Vine, F. J., and D. H. Matthews (1963), Magnetic anomalies over oceanic ridges, *Nature*, *199*, 947–949, doi:10.1038/199947a0.

Wallick, B. P., and M. B. Steiner (1982), Paleomagnetic and rock magnetic properties of Jurassic Quiet Zone basalts, Hole 801C, *Proc. ODP Sci. Res.*, *129*, 455–470.

S.-M. Lee, School of Earth and Environmental Science, Seoul National University, Gwanak-gu Sillim-dong, Seoul 151-747, Korea.

W. W. Sager and M. Tominaga, Department of Oceanography, Texas A&M University, College Station, TX 77843, USA. (mtominaga@ocean.tamu.edu; wsager@ocean.tamu.edu)

M. A. Tivey, Department of Geology and Geophysics, Woods Hole Oceanographic Institution, Woods Hole, MA 02543, USA. (mtivey@whoi.edu)